Microfluid Nanofluid (2012) 12:431–449
DOI 10.1007/s10404-011-0886-2

RESEARCH PAPER

Forced convection in electro-osmotic/Poiseuille micro-channel flows of viscoelastic fluids: fully developed flow with imposed wall heat flux

P. M. Coelho · M. A. Alves · F. T. Pinho

Received: 23 February 2011 / Accepted: 20 September 2011 / Published online: 16 October 2011

Abstract The analytical solution for heat transfer in a dynamic and thermally fully developed channel flow of the simplified Phan-Thien–Tanner fluid induced by combined electro-osmosis and pressure gradient was obtained assuming that material properties are independent of temperature. The flow forcing was quantified by an appropriate dimensionless parameter and its effect and that of all other relevant dimensionless numbers is presented and discussed. Specifically, the forced convection occurs under conditions of constant wall heat flux and the solution includes the effects of Weissenberg number, electric double layer (EDL) thickness, forcing ratio parameter, viscous dissipation as well as of Joule heating due to the electric currents and was obtained under the simplifying Debye–Hückel approximation. Generally speaking, the Joule effect is stronger than the viscous dissipation except in very narrow channels, but these fall outside the validity of the Debye–Hückel conditions. For pure electro-osmosis, viscous dissipation is restricted to the near-wall region and virtually nonexistent elsewhere, so it is irrelevant for thin electric double layers and Joule heating is more relevant. As the EDL thickens and/or the pressure gradient contribution increases, the role of viscous dissipation grows and shear-thinning effects also appear more clearly on the Nusselt number. Generally speaking, an increase in internal heating results in lower Nusselt numbers and this effect is stronger than the effect of shear-thinning, which is responsible for a slight increase in the Nusselt number.

Keywords Viscoelastic fluid · sPTT model · Electro-osmosis · Constant wall heat flux · Nusselt number · Analytical solution

P. M. Coelho · F. T. Pinho (✉)
Departamento de Engenharia Mecânica, Centro de Estudos de Fenómenos de Transporte, Faculdade de Engenharia da Universidade do Porto, Rua Dr. Roberto Frias s/n, 4200-465 Porto, Portugal
e-mail: fpinho@fe.up.pt

P. M. Coelho
e-mail: pmc@fe.up.pt

M. A. Alves
Departamento de Engenharia Química, Centro de Estudos de Fenómenos de Transporte, Faculdade de Engenharia da Universidade do Porto, Rua Dr. Roberto Frias s/n, 4200-465 Porto, Portugal
e-mail: mmalves@fe.up.pt

List of symbols

Abbreviations

Br	Brinkman number, $Br = \tau_{w,p}\bar{u}/8\dot{q}_w$ (–)
c	Specific heat (J kg^{-1} K^{-1})
D_h	Hydraulic diameter, $D_\mathrm{h} = 4H$ (m)
e	Elementary electronic charge (1.6022×10^{-19} C)
EDL	Electrical double layer
E_x	x-component of the applied electrical field (V m^{-1})
h	Convective heat transfer coefficient (W m^{-2} K^{-1})
H	Micro-channel half-height (m)
H^+	Channel height normalized by the Debye layer thickness, $H^+ = H\kappa$ (–)
Jo	Joule number, $Jo = \sigma E_x^2 D_\mathrm{h}/\dot{q}_w$ (–)
k_B	Boltzmann constant (1.3807×10^{-23} J K^{-1})
k_th	Thermal conductivity of the fluid (W m^{-1} K^{-1})
n_o	Ionic density (m^{-3})
Nu	Nusselt number, $Nu = h D_\mathrm{h}/k_\mathrm{th}$ (–)
Pe	Péclet number, $Pe = RePr = \rho u D_\mathrm{h} c/k_\mathrm{th}$ (–)
Pr	Prandtl number, $Pr = \eta c/k_\mathrm{th}$ (–)
p	Pressure (Pa)
$p_{,x}$	Pressure gradient, $p_{,x} = \mathrm{d}p/\mathrm{d}x$ (Pa m^{-1})

$\dot{q}$ Joule heating per unit volume (W m^{-3})
$\dot{q}_w$ Wall heat flux (positive if transferred to the fluid) (W m^{-2})
Re Reynolds number $Re = \rho \bar{u} D_h/\eta$ (–)
T Absolute temperature (K)
T^+ Normalized temperature difference, $T^+ = (T - T_0)/(\dot{q}_w D_h/k_{th})$ (–)
$\bar{T}^+$ Average normalized temperature difference (–)
T_w^+ Normalized wall temperature difference (–)
T_0 Reference temperature (a constant value such as an inlet bulk temperature) (K)
u Stream-wise velocity (m s^{-1})
$\bar{u}$ Average velocity for the sPTT fluid (m s^{-1})
u_{sh} Helmholtz–Smoluchowski electro-osmotic velocity $u_{sh} = -\in \psi_0 E_x/\eta$ (m s^{-1})
u_N Average velocity for fully developed Poiseuille flow of a Newtonian fluid subjected to the same pressure gradient, $u_N = -H^2 p_{,x}/3\eta$ (m s^{-1})
u^+ Stream-wise velocity normalized by the bulk velocity, $u^+ = u/\bar{u}$ (–)
w Micro-channel width, $w \gg 2H$ (m)
Wi Weissenberg number, $Wi = \lambda \bar{u}/H$ (–)
Wi_κ Weissenberg number, $Wi_\kappa = \lambda \kappa u_{sh}$ (–)
Wi_N Weissenberg number, $Wi_N = \lambda u_N/H = -Wi_\kappa \Gamma/(3H^+)$ (–)
x Stream-wise coordinate (m)
x' Normalized stream-wise coordinate, $x' = x/(D_h\, Re\, Pr)$ (–)
y Transverse coordinate (m)
y^+ Transverse coordinate normalized by the Debye layer thickness, $y^+ = y\kappa$ (–)
z Valence of the ions (–)

Tensors and vectors

D Rate of deformation tensor (s^{-1})
E Applied external electric field (V m^{-1})
u Velocity vector (m s^{-1})
$\boldsymbol{\tau}$ Polymeric extra-stress tensor (Pa)

Greek symbols

$\dot{\gamma}$ Velocity gradient, $\mathrm{d}u/\mathrm{d}y$ (s^{-1})
$\dot{\gamma}^+$ Normalized velocity gradient, $\mathrm{d}u^+/\mathrm{d}y^+$ (–)
Γ Dimensionless ratio between electro-osmosis and pressure gradient forcings, $\Gamma = -H^2 p_{,x}/(\in \psi_0 E_x) = -3u_N/u_{sh}$ (–)
ε Extensibility parameter of the sPTT model (–)
$\in$ Permittivity of the solution, the product of the dimensionless dielectric constant by the vacuum permittivity (C V^{-1} m^{-1})
$\in_r$ Dielectric constant of the solution, the ratio between the permittivities of the solution and vacuum (–)
ϕ Imposed potential field (V)
η Polymer viscosity coefficient (Pa s)
λ Relaxation time (s)
ψ Induced potential field (V)
ψ_o Zeta (wall) potential (V)
κ^2 Debye–Hückel parameter (m^{-2})
ξ Debye layer thickness (also referred to as the EDL thickness), $\xi = 1/\kappa$ (m)
ρ Fluid density (kg m^{-3})
ρ_e Net electrical charge density in the fluid (C m^{-3})
σ Electrical conductivity of the liquid (Ω^{-1} m^{-1})
τ_{xy} Shear stress (Pa)
τ_{xy}^+ Normalized shear stress, $\tau_{xy}^+ = \tau_{xy}/\tau_{w,p}$ (–)
$\tau_{w,p}$ Particular wall shear stress (defined in Eq. 24) (Pa)

1 Introduction

The advent of new micro-manufacturing techniques has fostered the development of microfluidic systems and their industrial application in a variety of systems and processes is gaining momentum (Stone et al. 2004). Examples go from separation processes in biofluids to dewatering of kelp or cooling of microelectronic components, amongst others. As the flow systems are miniaturized, the overall impact of surface forces increases in detriment of volume forces (Stone et al. 2004; Bruus 2008); hence, electrokinetic or capillary effects, which are usually negligible in macro-processes, can dominate the flow characteristics. In addition, the earlier development of micro-electronics allows today for the integration of electric and flow systems at the micro-scale, hence electrokinetics is bound to be ever more frequent as a forcing flow mechanism in microfluidics, while preserving a low cost for the miniaturized systems.

Electrokinetic effects can exist when dielectric surfaces are brought in contact with polar fluids and are exploited by the application of external electric potentials in the flow direction as well as by adequate modifications of the spontaneous wall potentials (Park and Choi 2009). Electro-osmosis and electrophoresis are commonly used to separate and synthesize biological and chemical components as in the separation and manipulation of DNA molecules, biopolymers and large proteins (Jendrejack et al. 2003, Berthier and Silberzan 2006). These and other biofluids are complex fluids containing macromolecules and consequently possess a complex rheology characterized by shear-thinning viscosity, viscoelasticity, thixotropy and yield stress, in isolation, but most often in combination (Larson 1999).

Theoretical studies of electro-osmosis of non-Newtonian fluids are very recent and mostly concerned with inelastic rheological constitutive equations. The common model for most existing studies is the Generalized Newtonian Fluid

(GNF) model with a power law viscosity function. This is a purely viscous model unable to predict viscoelastic fluid flow features such as memory effects or shear-induced normal stresses in general flows. Additionally, the power law model only captures the variable viscosity typical of intermediate shear rates, while most non-Newtonian fluids are characterized by a constant viscosity plateau at low shear rates. These various features are captured by some viscoelastic differential constitutive equations, such as the Phan-Thien–Tanner model (Bird et al. 1987). Therefore, only when the relevant flow shear rates are well beyond the constant viscosity plateau and in the absence of time effects (fully developed flow), the power law model will provide a good approximation to the velocity profile of the viscoelastic fluid. Das and Chakraborty (2006) and Chakraborty (2007) obtained analytical solutions for velocity, temperature and concentration distributions in electro-osmotic micro-channel flows for power law fluids and for blood flow. Chakraborty (2005) used the same constitutive equation in spite of the evidence that blood has other non-Newtonian characteristics, which are especially strong in small blood vessels (Easthope and Brooks 1980; Dutta and Tarbell 1996; Moyers-Gonzalez et al. 2008). Other purely viscous models were analytically investigated by Berli and Olivares (2008), who considered, amongst other things, the effect upon the flow characteristics of the existence of a wall layer depleted of macromolecules. These theoretical results have also been validated by experimental data by Olivares et al. (2009), who investigated the flow of carboxymethyl cellulose (CMC) solutions in fused silica capillaries.

For viscoelastic rheological constitutive equations Park and Lee (2008) deduced the Helmholtz–Smoluchowski velocity for fluids described by several forms of the Phan-Thien–Tanner model, including its simplified version, and provided a simple procedure to numerically calculate its value. Afonso et al. (2009) derived analytically the velocity profile for fully developed channel flow of sPTT fluids under combined electro-osmotic/pressure gradient forcing, including the quantification of the streaming potential. In contrast to the Newtonian fluid case, they showed that for the sPTT fluid the solution is not just the result of a linear superposition of the pure Poiseuille and pure electro-osmotic flows, but includes a non-linear term proportional to both forcing mechanisms. It is important to realize that the viscoelastic results of Afonso et al. (2009), and those of many earlier works for Newtonian and non-Newtonian fluids, were obtained under simplified conditions, where the induced electric potential was governed by a linear form of the so-called Poisson–Boltzmann equation. More recently, Sousa et al. (2011) extended this solution of Afonso et al. (2009) to include the effect of a Newtonian skimming layer near the wall. When this electric double layer (EDL) is much thinner than the skimming layer, the flow is essentially controlled by the Newtonian fluid occupying this skimming layer and the flow characteristics are identical to what would be obtained if the whole channel was to be occupied by the Newtonian fluid. However, when the thickness of the skimming and EDL layers approach each other and/or the pressure forcing is large relative to the electro-osmotic forcing, the rheology of the non-Newtonian fluid in the bulk cannot be neglected.

Promising applications of these systems involve cooling or heating, such as in the cooling of microchips, therefore heat transfer is an important process at the microscale. Miniaturization is changing the design of heat exchangers. These have evolved from the classical designs to compact plate heat exchangers with channels of 3–10 mm size and now the advent of cheap micro-manufacturing is leading the industry to the production of highly compact heat exchangers with micro-channels of the order of 100–300 μm, which are characterized by very high heat transfer coefficients and low pressure drops. These will increasingly be used to deal with a variety of complex and synthetic fluids, such as biofluids or fluids for the food industry, which exhibit viscoelastic rheology and it is only a matter of time for the miniaturized heat exchangers to adopt forcing by electro-osmosis for certain applications, since it can be more efficient than pressure forcing at very small scales.

The small sizes involved can make internal viscous dissipation an important part of these processes, but in addition the presence of an electric current also induces heating by the Joule effect. Research on heat transfer in micro-channels in the presence of electro-osmosis was carried out by Mala et al. (1997) and Yang et al. (1998) for fully developed flow, the former for weak wall potentials, the latter for strong wall potentials. Note that for weak wall potentials a simpler solution is obtained by using a linearization, known as the Debye–Hückel approximation (cf. Debye and Hückel 1923). Soong and Wang (2003) extended the weak wall potential solution to deal with asymmetric wall conditions for both the wall potential and the wall heat transfer, a common situation in micro-manufacturing, where channels often have opposite walls made of different materials Nguyen and Wereley (2006). These early works did not include the effect of viscous dissipation, which was extensively investigated by Koo and Kleinstreuer (2004) to conclude that it should not be neglected for liquid flows in channels smaller than about 50 μm in thickness. Viscous dissipation can be very important even at low Reynolds number flows, when the fluids have a large viscosity (a feature of many viscoelastic fluids) and when the aspect ratio of the duct deviates from unity, the case of a channel flow.

For high zeta potentials, the solution is more elaborate and sometimes it is only semi-analytical given the non-linear nature of the equation governing the induced electric potential. Very recently, a heat transfer solution was obtained for the parallel-plate micro-channel flow of Newtonian fluids by Elazhary and Soliman (2009), considering also the effect of viscous dissipation. They compared it with the simpler solution based on the linearized Poisson–Boltzmann equation, but the Joule heating effect was not accounted for in any of their results.

A mathematical model was developed by Tang et al. (2003) to investigate the effect of Joule heating in pure electro-osmosis and capillary electrophoresis for Newtonian fluids including the conjugate wall heat conduction. Here, the fluid properties were made to depend on fluid temperature and consequently the governing equations were solved numerically, showing non-negligible effects of Joule heating on fully developed channel flow. Assuming temperature-independent fluid properties and very thin electric double layers (plug velocity profiles), Horiuchi and Dutta (2004) were able to derive analytical solutions for the flow heat transfer problem for imposed constant surface temperature as well as constant wall heat flux, but neglecting viscous dissipation. These authors also showed that viscous dissipation was important for small channels (less than 20 μm thick), but negligible otherwise, whereas Joule heating effects would be enhanced as the channel thickness increased since it is a volume effect. In fact, the more detailed numerical investigations of Tang et al. (2004) on the effect of Joule heating with temperature-dependent viscosity showed increases of more than 70% in the pure electro-osmotic velocity for fully developed flow in a 200-μm-thick channel relative to the Helmholtz–Smoluchowski velocity for temperature-independent viscosity and no Joule heating, whereas for a 50-μm channel the increase was only 5%. These authors also showed that under high electric field strengths, temperature changes due to Joule heating can be sufficiently high to vaporize the liquid inside the channels. The subsequent experiments of Tang et al. (2006) using PDMS channels validated some of their earlier findings.

All of the above heat transfer works pertain to Newtonian fluids, and extensions for non-Newtonian fluids are scarce. Das and Chakraborty (2006) did it for inelastic power law non-Newtonian fluids, but heat transfer investigations for viscoelastic fluids in the presence of electro-osmosis have yet to be carried out.

In this work we investigate analytically the heat transfer of viscoelastic fluids, described by the simplified Phan-Thien–Tanner model, in dynamic and thermally fully developed channel flow forced by a combination of electro-osmosis and pressure gradient under conditions of constant wall heat flux, including the effects of viscous dissipation and the most relevant effects of Joule heating. The flow geometry, its dimensions and the coordinate system used are schematically shown in Fig. 1.

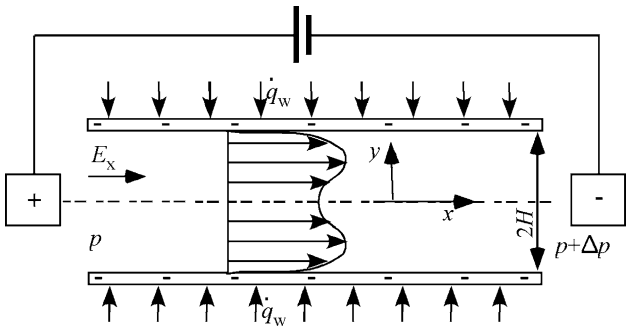

Fig. 1 Schematic representation of the flow geometry and coordinate system

The next section presents the governing equations, followed by the definition of all relevant non-dimensional quantities and ends with the presentation of the normalized equations. Then, the heat transfer solution is presented in Sect. 3 and results are discussed in Sect. 4 prior to a summary of the main conclusions.

2 Governing equations

A general problem of forced convection requires the simultaneous solution of the equations governing mass conservation, momentum and thermal energy, in addition to the rheological constitutive equation, even under fully developed conditions. If the flow is forced by electrokinetic effects, the momentum equation is modified to include the electric force and it is also necessary to include the equations governing the distribution of ions due to flow transport and the total electric potential (the Nernst–Planck equations), the equation governing the induced electric potential (the Poisson equation) and the definition of the net electric charge. Under certain conditions, such as in fully developed channel flow where the electric double layers are in equilibrium, the Nernst–Planck equations simplify to the Boltzmann distribution and the induced potential and electric charge distribution can be calculated by the so-called Poisson–Boltzmann model.

Now, if the assumption is made that all model parameters are independent of temperature, the dynamic solution and the solution of the Poisson–Boltzmann equation become decoupled from the thermal solution and can be obtained separately as in isothermal flow. This assumption is here invoked limiting the temperature differences to small values, but it is also one of convenience, since an analytical solution would not be possible with the fully coupled problem. The fluid properties most affected by

temperature are the polymer viscosity and the permittivity of the medium. The viscoelastic polymer solutions used in micro-channels are usually based on water for which the viscosity has a variation of approximately 2%/K. Catenaccio et al. (2003) report for the permittivity of water a dependence of the order of 0.5%/K, i.e., four times lower. Therefore, the small temperature difference required for the validity of the analytical solution is mostly imposed by the viscosity. Hence, this analytical solution should also be viewed as an approximation to the exact solution for large temperature differences. As such, it will also allow in a simple manner to identify the correct trends and the role of all relevant quantities in a more complex setting.

The problem under analysis is that of forced convection in fully developed channel flow of viscoelastic fluids forced by electro-osmosis and pressure gradient. The fluids are described by the simplified version of the Phan-Thien–Tanner model (sPTT), and the assumption of temperature-independent fluid properties makes the isothermal flow solution of Afonso et al. (2009) as the fluid dynamic solution for this problem. All assumptions invoked by Afonso et al. (2009) must also apply here. These are the validity of the so-called standard electrokinetic model and the Debye–Hückel approximation of the Poisson–Boltzmann potential model, as briefly explained below. Full details are given in Afonso et al. (2009).

2.1 Equations governing isothermal flow

The equations solved by Afonso et al. (2009) for fully developed channel flow were the mass conservation (Eq. 1) and momentum (Eq. 2) equations:

$$\nabla \cdot \mathbf{u} = 0 \tag{1}$$

$$-\nabla p + \nabla \cdot \boldsymbol{\tau} + \rho_e \mathbf{E} = \mathbf{0}, \tag{2}$$

where $\mathbf{u}$ is the velocity vector, p is the pressure and $\boldsymbol{\tau}$ is the polymeric extra-stress tensor contribution. The body force per unit volume of electro-osmosis is $\rho_e \mathbf{E}$, where $\mathbf{E} = -\nabla\phi$ is the applied external electric field (ϕ is the corresponding imposed electric potential) and ρ_e is the net electric charge density in the fluid, which here depends only on the induced electric potential (in general it depends on the total electric potential).

The polymer stress is given by the sPTT rheological constitutive equation,

$$f(\mathrm{tr}\boldsymbol{\tau})\boldsymbol{\tau} + \lambda \overset{\nabla}{\boldsymbol{\tau}} = 2\eta \mathbf{D}, \tag{3}$$

where the rate of deformation tensor is $\mathbf{D} = (\nabla \mathbf{u}^T + \nabla \mathbf{u})/2$, λ is the fluid relaxation time, η is the polymer viscosity coefficient and $\overset{\nabla}{\boldsymbol{\tau}}$ represents the upper-convected derivative of $\boldsymbol{\tau}$:

$$\overset{\nabla}{\boldsymbol{\tau}} = \frac{\mathrm{D}\boldsymbol{\tau}}{\mathrm{D}t} - \nabla \mathbf{u}^T \cdot \boldsymbol{\tau} - \boldsymbol{\tau} \cdot \nabla \mathbf{u}. \tag{4}$$

The function of the trace in Eq. 3 is given by the linear form,

$$f(\mathrm{tr}\,\boldsymbol{\tau}) = 1 + \frac{\varepsilon\lambda}{\eta}\mathrm{tr}\,\boldsymbol{\tau} \tag{5}$$

introducing parameter ε, which imposes an upper limit to the extensional viscosity.

In steady fully developed channel flow, convective terms are null, including those in the Nernst–Planck equations governing the transport of ions, thus implying that there is equilibrium in the ionic distribution in the thin electric double layer (EDL) forming spontaneously near the dielectric walls (Russel et al. 1991). As a consequence, the Nernst–Planck equations are well approximated by the Boltzmann distribution (Tang et al. 2003; Park et al. 2007; Park and Choi 2009), where the net electric charge density for an electrolyte solution in equilibrium near a charged surface is determined by:

$$\rho_e = -2n_0 ez \sinh\left(\frac{ez}{k_\mathrm{B}T}\psi\right) \rightarrow \rho_e \approx -2n_0 \frac{e^2z^2}{k_\mathrm{B}T}\psi, \tag{6}$$

and the induced potential is given by the Poisson equation

$$\nabla^2\psi = -\frac{\rho_e}{\in}. \tag{7}$$

In this Poisson–Boltzmann model ψ is the induced potential at the EDL, $\in$ is the permittivity of the fluid, n_0 is the ionic density, e is the elementary charge and z is the valence of the ions. It is also assumed that the gradient of the induced electric potential is much larger than the gradient of the imposed electric potential, a feature of the so-called standard electrokinetic theory (Afonso et al. 2009).

In their solution of the Poisson–Boltzmann model, Afonso et al. (2009) finally invoked the Debye–Hückel approximation (Debye and Hückel 1923), which is only valid for weak wall potentials (approximately <26 mV for monovalent ions and <13 mV for divalent electrolytes) in order to have a small value of $ez\psi/k_\mathrm{B}T$. This allows the linearization of the hyperbolic sine function [$\sinh(x) \approx x$] and leads to the simplified expression on the right-hand side of Eq. 6.

Afonso et al. (2009) presented the fully developed solution for combined electro-osmosis/Poiseuille flow of sPTT fluids in dimensional and dimensionless form by providing expressions for the velocity profile (u), the velocity gradient ($\dot{\gamma}$), the shear stress (τ_{xy}), and for the distributions of the induced potential (ψ) and of the net electric charge density (ρ_e). However, the use of their dimensionless solution leads to a more complex heat

transfer analytical solution, so in this work we normalize the dynamic solution differently, as explained in detail in Sect. 2.4.

2.2 Heat transfer governing equation

Only the thermal energy transport equation needs to be solved, which for dynamic and thermally fully developed steady channel flow is

$$\rho c\,\mathbf{u}\cdot\nabla T=\nabla\cdot(k_{\mathrm{th}}\nabla T)+\boldsymbol{\tau}:\mathbf{D}+\dot{q} \tag{8}$$

where k_{th} is the thermal conductivity of the fluid, $\boldsymbol{\tau}$:$\mathbf{D}$ represents the viscoelastic stress work and $\dot{q}$ is a source, here representing Joule heating per unit volume. Under these fully developed flow conditions, the viscoelastic stress work becomes the viscous dissipation (often denoted as Φ), which simplifies to $\Phi=\boldsymbol{\tau}:\mathbf{D}=\tau_{xy}\dot{\gamma}$. Even though for general flows of viscoelastic fluids the thermal energy equation has extra terms related to the rheological equation, it reduces to this form under fully developed conditions (cf. Wapperom and Hulsen 1998; Pinho and Coelho 2006).

The Joule heating effect is a consequence of the application of an electric field across a conductive fluid and is given in complete form as:

$$\dot{q}=\frac{1}{\sigma}(\rho_e\mathbf{u}+\sigma\mathbf{E})\cdot(\rho_e\mathbf{u}+\sigma\mathbf{E}), \tag{9}$$

where σ represents the electrical conductivity of the fluid.

However, we neglect the convective contribution in comparison to the electric conduction contribution as was done by Das and Chakraborty (2006). To show that the contribution of the velocity field to the Joule heating is negligible in comparison with the direct effect of the imposed electrical field, consider fully developed channel flow, the velocity is of the order of the Helmholtz–Smoluchowski velocity and that the net electric charge density takes the maximum value allowed here by the validity of the Debye–Hückel approximation ($ez\psi_0/k_{\mathrm{B}}T\sim 1$ and consequently $\psi_0\approx 26$ mV for water). In addition, consider also typical values of other properties for water at 20°C ($\eta=0.001$ Pa s, $\epsilon_r=80$) and a solute concentration of 1 mM ($n_0=6.022\times 10^{23}$ m^{-3}) to arrive at

$$\left(\frac{\rho_e u}{\sigma E_x}\right)^2\approx\left[\frac{2\sigma e n_0\sinh(1)\frac{\in\psi_0 E_x}{\eta}}{\sigma E_x}\right]^2\approx\left(\frac{2e n_0\in\psi_0}{\eta}\right)^2\sim 10^{-5} \tag{10}$$

The numerical calculations of Tang et al. (2004) confirmed this conclusion without invoking the Debye–Hückel approximation, and considering also the effects of temperature on flow properties and higher concentrations of solute. Hence, we use the following equation for the Joule heating effect:

$$\dot{q}=\sigma\mathbf{E}\cdot\mathbf{E}=\sigma E_x^2 \tag{11}$$

To integrate the thermal energy equation the following two boundary conditions are used: constant wall heat flux ($\dot{q}_w$ at $y=\pm H$) and the symmetry condition on the centreline ($\partial T/\partial y|_{y=0}=0$).

2.3 Relevant dimensionless numbers and normalized energy equation

For the sake of generality we work with the normalized form of the energy equation and present the results in dimensionless form. Here, we do not use exactly the normalization introduced by Afonso et al. (2009), which is based on the Helmholtz–Smoluchowski velocity as a velocity scale, but instead rely on a mixture of velocity scales, including also the bulk velocity. This has advantages regarding the heat transfer solution, the physical interpretation of its results and the use of some dimensionless numbers directly related to heat transfer, such as the unified Brinkman number (Coelho and Pinho 2009). The dimensionless temperature (T^+), transverse coordinate (y^+), stream-wise coordinate (x'), shear stress (τ_{xy}^+) and stream-wise velocity (u^+) are defined as:

$$T^+=\frac{T-T_0}{\dot{q}_w D_{\mathrm{h}}/k_{\mathrm{th}}},\ y^+=y\kappa,\ x'=\frac{x}{D_{\mathrm{h}}\,Re\,Pr},\qquad \tau_{xy}^+=\frac{\tau_{xy}}{\tau_{w,p}},\ u^+=\frac{u}{\bar{u}} \tag{12}$$

where $\bar{u}$ stands for the flow area-averaged velocity (also denoted as bulk velocity), D_{h} is the channel hydraulic diameter ($D_{\mathrm{h}}=4H$), T_0 is a reference temperature, which was taken to be inlet bulk temperature (it can be any constant temperature value) and $\tau_{w,p}$ is a very particular shear stress to be defined below. The Reynolds and Prandtl numbers are defined as $Re=\rho\,\bar{u}\,D_{\mathrm{h}}/\eta$ and $Pr=\eta\,c/k_{\mathrm{th}}$, respectively, and their product is the viscosity-independent Péclet number, $Pe=\rho\,\bar{u}\,D_{\mathrm{h}}c/k_{\mathrm{th}}$.

The solution, given in terms of these dimensionless quantities, is also a function of various other non-dimensional numbers; some appear through the fluid dynamic solution, namely the group $\varepsilon\,Wi_\kappa^2$ related to fluid non-linearity, where the Weissenberg number (Wi_κ) is the product of the fluid relaxation time by a characteristic flow shear rate based on the Helmholtz–Smoluchowski velocity ($u_{\mathrm{sh}}=-\in\psi_0E_x/\eta$) and on the EDL thickness (Afonso et al. 2009), whereas others originate in the thermal energy equation. In this second group of dimensionless numbers we emphasize the unified Brinkman number (Br) (Coelho and Pinho 2009), relating the energy generated internally

by the viscous stress work with the heat flux at the wall and the Joule number (Jo) relating the heat generated internally by the Joule heating effect with the wall heat flux (Tang et al. (2006) defined alternatively the Joule number as the non-dimensional ratio of Joule heating to diffusion heat transfer). All these quantities are defined as:

$$Wi_\kappa = \lambda\,\kappa\,u_{\rm sh},\; Br = \frac{\tau_{w,p}\,\bar{u}}{8\,\dot{q}_{\rm w}},\; Jo = \frac{\sigma\,E_x^2\,D_{\rm h}}{\dot{q}_{\rm w}} \text{ and } Wi_N = \frac{\lambda u_N}{H}. \tag{13}$$

An additional Weissenberg number (Wi_N) defined in Eq. 13 is also used and relates the relaxation time, the channel half-height (H) and an equivalent Newtonian velocity to be defined below. As will be further discussed, it can be used as a complement to Wi_κ and there is a third Weissenberg number (Wi) that can be used as an alternative, which uses the bulk velocity as the velocity scale, $Wi = \lambda\bar{u}/H$. This is the standard definition in pressure-based flows. From a physical point of view a single Weissenberg number is required and the usual definition is this last one, $Wi = \lambda\bar{u}/H$. However, the analytical form of the thermal solution to be derived would be extremely more complex if cast in terms of Wi instead of relying on both Wi_κ and Wi_N for simplicity. Note also that in their previous work Afonso et al. (2009) called the non-dimensional groups built with the relaxation time as Deborah numbers, but since this is a steady flow the correct interpretation is that of a Weissenberg number, the designation used throughout this paper.

These non-dimensional parameters can be positive or negative, depending on the signs of $u_{\rm sh}$ and $\dot{q}_w$. A positive $\dot{q}_{\rm w}$ is assumed when the heat is transferred to the fluid and negative when there is surface cooling.

After simplification and normalization, the dimensionless thermal energy equation that needs to be integrated becomes

$$\frac{\partial^2 T^+}{\partial y^{+2}} + \frac{8Br}{\kappa D_h}\tau_{xy}^+\frac{{\rm d}u^+}{{\rm d}y^+} + \frac{Jo}{\kappa^2 D_h^2} = \frac{u^+}{\kappa^2 D_h^2}\frac{\partial T^+}{\partial x'} \tag{14}$$

subject to boundary conditions $T^+ = T_w^+$ at $y^+ = H^+$ and $\partial T^+/\partial\, y^+|_{y^+=0} = 0$, where $H^+ = \kappa H$ (or $H^+ \equiv \bar{\kappa}$ as used by Afonso et al. 2009). It is important to realize that T_w^+ varies along the wall and that normalizing the wall heat flux boundary condition ($k_{\rm th}\partial T/\partial y|_{y=H} = \dot{q}_w$) leads to $(\partial T^+/\partial\, y^+)|_{y^+=H^+} = 1/(\kappa D_{\rm h}) = 1/(4H^+)$, a result that can be used to confirm the equation for $\partial T^+/\partial y^+$ that will be obtained from integration of Eq. 14.

2.4 Normalized flow solution and relevant dimensionless numbers

The solution for viscoelastic flow depends on three independent dimensionless numbers as shown by Afonso et al. (2009). They used H^+, which was represented as $\bar{\kappa}$, $\sqrt{\varepsilon}\,Wi_\kappa$, and the non-dimensional ratio of the electro-osmosis and pressure gradient forcings $\Gamma = -H^2 p_{,x}/(\in \psi_0 E_x)$. Here we will use the same set of dimensionless numbers, except for the limiting condition of pure Poiseuille flow. Regarding the velocity profile, Afonso et al. (2009) normalized it by the Helmholtz–Smoluchowski velocity, which is inconvenient for the same limiting case. To avoid this and also arrive at a more compact expression than Afonso et al. (2009), which simplifies the heat transfer solution, we renormalize their velocity profile by the bulk velocity of the sPTT fluid ($\bar{u}$) and additionally, we use the equivalent Newtonian bulk velocity (u_N) that would be observed for the corresponding flow of a Newtonian fluid under the sole influence of a pressure gradient, $u_N = -H^2 p_{,x}/(3\eta)$, which actually leads to the second Weissenberg number (Wi_N) defined in Eq. 13. There is a relationship between those two Weissenberg numbers via the non-dimensional ratio between the electro-osmosis and pressure gradient forcings, Γ, which is $Wi_N = -Wi_\kappa\,\Gamma/(3H^+)$, that is equivalent to $u_N/u_{\rm sh} = -\Gamma/3$. In the analysis of the results in Sect. 4, we will use the non-dimensional number $\sqrt{\varepsilon}\,Wi_N$ as a measure of elasticity instead of $\sqrt{\varepsilon}\,Wi_\kappa$, when the latter and Γ both lose their significance, i.e. in the limit of pure Poiseuille flow, $\Gamma^{-1} \to 0$.

The integration of the velocity profile given by Afonso et al. (2009) leads to the following equation for the average velocity, $\bar{u}$:

$$\frac{\bar{u}}{u_{\rm sh}} = \frac{\alpha_1\cosh(3H^+) + \alpha_2\sinh(3H^+) + \alpha_3\cosh(2H^+) + \alpha_4\sinh(2H^+) + \alpha_5\cosh(H^+) + \alpha_6\sinh(H^+) + \alpha_7}{\alpha_8\cosh(H^+)} \tag{15}$$

with,

$$\alpha_1 = 60\,c_1^2(2H^{+^3} + 3\,\Gamma\,H^+)$$
$$\alpha_2 = -10\,c_1^2[2H^{+^2}(2+9\,\Gamma) + 9\,\Gamma];$$
$$\alpha_3 = -720\,c_1\,c_2\,H^+[H^{+2}(2\,\Gamma+1) + 12\,\Gamma]\,;$$
$$\alpha_4 = 360\,c_1\,c_2\,[2H^{+^4} + H^{+^2}(1+12\,\Gamma) + 24\,\Gamma];$$
$$\alpha_5 = 18\left\{16\,c_2^2H^{+5}(5-\Gamma) + 80H^{+3}(6\,c_2^2 + 1 - \Gamma/3)\right.$$
$$\left.-[20\,c_1^2H^{+3}(3-2\Gamma/3) - 10\,c_1^2H^+\Gamma]\right\};$$
$$\alpha_6 = 18\,[10\,c_1^2H^{+^2}(6-\Gamma) - 5\,c_1^2\,\Gamma - 240c_2^2H^{+^4}$$
$$-\,80\,H^{+^2}(1+6\,c_2^2)];$$
$$\alpha_7 = -480\,c_1\,c_2\,H^+(H^{+4} + 3H^{+2}\Gamma + 18\,\Gamma)$$
$$\text{and}\ \alpha_8 = 1440H^{+^3} \tag{16}$$

where,

$$c_1 = -\frac{\sqrt{2}}{\cosh(H^+)}\sqrt{\varepsilon}\,Wi_k;\ c_2 = \frac{\sqrt{2}\,\Gamma}{H^{+^2}}\sqrt{\varepsilon}\,Wi_k. \tag{17}$$

The velocity profile given by Afonso et al. (2009) and now normalized by this bulk velocity ($u^+ \equiv u/\bar{u}$) is written as

$$u^+ = \omega_1\cosh(3y^+) + \omega_2\,[2y^+\sinh(2y^+) - \cosh(2y^+)]$$
$$+\,\omega_3[y^{+^2}\cosh(y^+) - 2y^+\sinh(y^+)] - \omega_4\cosh(y^+)$$
$$-\,\omega_5\,y^{+2} + \omega_6\,y^{+4} + \omega_7 \tag{18}$$

with

$$\omega_1 = c_1^2c_3/12;\ \omega_2 = c_1(c_1c_4 + 2c_2c_3)/8;$$
$$\omega_3 = c_2(2c_1c_4 + c_2c_3)$$
$$\omega_4 = [3c_1^2c_3 - 16c_1c_2c_4 - 4c_3(1+2c_2^2)]/4;$$
$$\omega_5 = (c_1^2c_4 + 2c_1c_2c_3 - 2c_4)/4\,;$$
$$\omega_6 = c_2^2c_4/4$$
$$\omega_7 = -\omega_1\cosh(3H^+) - \omega_2\,[2H^+\sinh(2H^+) - \cosh(2H^+)]$$
$$-\,\omega_3\,[H^{+^2}\cosh(H^+) - 2H^+\sinh(H^+)]$$
$$+\,\omega_4\cosh(H^+) + \omega_5\,H^{+^2} - \omega_6\,H^{+^4} \tag{19}$$

and

$$c_3 = -\frac{u_{\rm sh}}{\bar{u}}\frac{1}{\cosh(H^+)};\ c_4 = \frac{\Gamma}{H^{+^2}}\frac{u_{\rm sh}}{\bar{u}} \tag{20}$$

The normalized transverse profile of velocity gradient can be written as (Afonso et al. 2009):

$$\dot{\gamma}^+ = \frac{\mathrm{d}u^+}{\mathrm{d}y^+}$$
$$= z_1\sinh(3y^+) + z_2\,y^+\cosh(2y^+)$$
$$-\left(z_3 + z_4\,y^{+^2}\right)\sinh(y^+) - y^+\left(z_5\,y^{+^2} + z_6\right) \tag{21}$$

with

$$z_1 = c_1^2c_3/4;\ z_2 = c_1\,c_2\,c_3 + c_1^2c_4/2;\ z_3 = c_3(3c_1^2 - 4)/4;$$
$$z_4 = -c_2(2c_1\,c_4 + c_2\,c_3);\ z_5 = -c_2^2\,c_4;$$
$$z_6 = (c_1^2\,c_4 + 2c_1\,c_2\,c_3 - 2c_4)/2 \tag{22}$$

where c_1, c_2 are given in Eq. 17 and c_3 and c_4 in Eq. 20.

Finally, to solve the energy Eq. 14 an expression for the non-dimensional shear stress is also necessary. The transverse profile of shear stress is given in Afonso et al. (2009), and its dimensionless form τ_{xy}^+ is here defined as

$$\tau_{xy}^+ = \frac{\tau_{xy}}{\tau_{w,p}} = \frac{1}{\tau_{w,p}}\left[\frac{p_{,x}}{\kappa}y^+ - \frac{\eta u_{\rm sh}\kappa}{\cosh(H^+)}\sinh(y^+)\right] \tag{23}$$

with $\tau_{w,p}$ defined as

$$\tau_{w,p} = \frac{1}{\bar{u}}\int_0^H \tau_{xy}\frac{\mathrm{d}u}{\mathrm{d}y}\mathrm{d}y = \int_0^{H^+}\tau_{xy}\frac{\mathrm{d}u^+}{\mathrm{d}y^+}\mathrm{d}y^+ \tag{24}$$

The product $2\tau_{w,p}\bar{u}$ is the power dissipation by viscous effects, and for Poiseuille flow it can be shown that $\tau_{w,p}$ corresponds to the wall shear stress. Integration of Eq. 24 leads to the following expression:

$$\frac{\tau_{w,p}}{\eta u_{\rm sh}\kappa} = -\frac{1}{8}\frac{z_1}{\cosh(H^+)}\sinh(4H^+)$$
$$+\frac{1}{6}\left[\frac{2\Gamma z_1}{H^{+^2}} - \frac{z_2}{\cosh(H^+)}\right]\left[H^+\cosh(3H^+) - \frac{\sinh(3H^+)}{3}\right]$$
$$+\frac{1}{8}\left[\frac{2H^{+^2}z_4}{\cosh(H^+)} + 4z_2\Gamma + \frac{2z_1}{\cosh(H^+)}\right.$$
$$\left.+\frac{2z_2\Gamma}{H^{+^2}} + \frac{2z_3+z_4}{\cosh(H^+)}\right]\sinh(2H^+)$$
$$-\frac{1}{4}\left[\frac{2\Gamma z_2}{H^{+^2}} + \frac{z_4}{\cosh(H^+)}\right]H^+\cosh(2H^+)$$
$$+\frac{1}{2}\left[6\Gamma z_4 - \frac{6H^{+^2}z_5}{\cosh(H^+)} + \frac{2\Gamma}{H^{+^2}}(z_3+6z_4)\right.$$
$$\left.-\frac{z_2+12z_5+2z_6}{\cosh(H^+)}\right]\sinh(H^+)$$
$$-\frac{1}{2}\left[2\Gamma z_4 - \frac{2H^{+^2}z_5}{\cosh(H^+)} + \frac{2\Gamma}{H^{+^2}}(z_3+6z_4)\right.$$
$$\left.-\frac{z_2+12z_5+2z_6}{\cosh(H^+)}\right]H^+\cosh(H^+).$$
$$-\frac{1}{30}\left\{H^{+^3}\left[6\Gamma z_5 + \frac{10\Gamma z_6}{H^{+^2}} + \frac{5z_4}{\cosh(H^+)}\right] + \frac{15H^+z_3}{\cosh(H^+)}\right\} \tag{25}$$

with coefficients z_1–z_6 given in Eq. 22.

3 Analytical solution for heat transfer

Integration of Eq. 14 from the centre plane to the wall,

$$\int_0^{H^+}\left(\frac{\partial^2 T^+}{\partial y^{+2}}+\frac{8Br}{\kappa D_h}\tau_{xy}^+\frac{du^+}{dy^+}+\frac{Jo}{\kappa^2 D_h^2}\right)dy^+ = \frac{1}{\kappa^2 D_h^2}\frac{\partial T^+}{\partial x'}\int_0^{H^+}u^+ dy^+ \tag{26}$$

leads to the following equation, that shows the stream-wise temperature gradient to be a constant, independent of y^+ as expected in thermally fully developed flow:

$$\frac{\partial T^+}{\partial x'}=\frac{d\bar{T}^+}{dx'}=4+Jo+32Br, \tag{27}$$

where $\bar{T}^+$ represents the mass-averaged temperature at a fixed x position, calculated by definition as:

$$\bar{T}^+=\frac{1}{H^+}\int_0^{H^+}u^+T^+dy^+. \tag{28}$$

To obtain Eq. 27 the boundary conditions $(\partial T^+/\partial y^+)|_{y^+=H^+}=1/(\kappa D_h)=1/(4H^+)$ and $(\partial T^+/\partial y^+)|_{y^+=0}=0$ were used, together with Eq. 24 ($\int_0^{H^+}\tau_{xy}^+(du^+/dy^+)dy^+=1$). It is also possible to arrive at Eq. 27 by an integral energy balance to the channel just invoking thermally and dynamically fully developed flow (heat input through the wall plus internal viscous dissipation and Joule heating equals internal energy increase). In any of the methods, $\partial T^+/\partial x'$ is then used to determine $\partial T^+/\partial y^+$ and the distribution of T^+ by successive integration of Eq. 14. The mass-weighted average temperature $\bar{T}^+$ is obtained from this transverse temperature distribution using Eq. 28.

The dimensionless temperature gradient can be computed from integration of Eq. 14 subject to the boundary condition $(\partial T^+/\partial y^+)_{y^+=0}=0$. This results in the following expression:

$$\begin{aligned}\frac{\partial T^+}{\partial y^+}=&\theta_1\sinh(4y^+)-\theta_2 y^+\cosh(3y^+)+\theta_3\sinh(3y^+)\\&+(\theta_4 y^{+2}+\theta_5)\sinh(2y^+)\\&+\theta_6 y^+\cosh(2y^+)+(\theta_7 y^{+^3}+\theta_8 y^+)\cosh(y^+)\\&-(\theta_9 y^{+^2}+\theta_{10})\sinh(y^+)\\&-\theta_{11}y^{+^5}-\theta_{12}y^{+^3}-\theta_{13}y^+\end{aligned} \tag{29}$$

with coefficients θ_1–θ_{13} given in Eq. 38 of the "Appendix".

We note that Eq. 29 verifies the condition $(\partial T^+/\partial y^+)|_{y^+=H^+}=1/(\kappa D_h)$, which can be obtained from normalization of $k_{th}\partial T/\partial y|_{y=H}=\dot{q}_w$, as explained in Sect. 2.3. Integrating the temperature gradient of Eq. 29 and applying the boundary condition $T^+=T_w^+$ at $y^+=H^+$ allows the determination of the dimensionless temperature profile:

$$T_w^+-T^+=f(H^+)-f(y^+) \tag{30}$$

where

$$\begin{aligned}f(y^+)=&\frac{\theta_1}{4}\cosh(4y^+)+\Upsilon_1\cosh(3y^+)\\&-\frac{\theta_2 y^+}{3}\sinh(3y^+)+\left(\frac{\theta_4 y^{+2}}{2}+\Upsilon_2\right)\cosh(2y^+)\\&+\Upsilon_3 y^+\sinh(2y^+)-\left(\Upsilon_4 y^{+2}+\Upsilon_5\right)\cosh(y^+)\\&+\left(\theta_7 y^{+2}+\Upsilon_6\right)y^+\sinh(y^+)\\&-\frac{y^{+2}}{12}\left(2\theta_{11}y^{+4}+3\theta_{12}y^{+2}+6\theta_{13}\right)\end{aligned} \tag{31}$$

and

$$\begin{aligned}&\Upsilon_1=\frac{\theta_2+3\theta_3}{9};\ \Upsilon_2=\frac{\theta_4+2\theta_5-\theta_6}{4};\ \Upsilon_3=\frac{\theta_6-\theta_4}{2};\\&\Upsilon_4=3\theta_7+\theta_9;\\&\Upsilon_5=6\theta_7+\theta_8+2\theta_9+\theta_{10};\ \Upsilon_6=\Upsilon_5-\theta_{10}\end{aligned} \tag{32}$$

Since the wall heat flux ($\dot{q}_w$) is imposed, and by definition

$$\dot{q}_w=h(T_w-\bar{T}), \tag{33}$$

where h represents the convective heat transfer coefficient and the two temperatures are at the same stream-wise position, the Nusselt number can be determined as,

$$Nu\equiv\frac{hD_h}{k_{th}}=\frac{1}{T_w^+-\bar{T}^+} \tag{34}$$

with the dimensionless temperature difference being defined as

$$T_w^+-\bar{T}^+=\frac{1}{H^+}\int_0^{H^+}u^+\left(T_w^+-T^+\right)dy^+ \tag{35}$$

and given by the following expression:

$$\begin{aligned}T_w^+-\bar{T}^+=&\Omega_1\sinh(7H^+)+\Omega_2\cosh(6H^+)\\&+\Omega_3\sinh(6H^+)+\Omega_4\cosh(5H^+)\\&+\Omega_5\sinh(5H^+)+\Omega_6\cosh(4H^+)\\&+\Omega_7\sinh(4H^+)+\Omega_8\cosh(3H^+)\\&+\Omega_9\sinh(3H^+)+\Omega_{10}\cosh(2H^+)\\&+\Omega_{11}\sinh(2H^+)+\Omega_{12}\cosh(H^+)\\&+\Omega_{13}\sinh(H^+)+\Omega_{14}\end{aligned} \tag{36}$$

with coefficients Ω_1–Ω_{14} given in Eq. 40 of the "Appendix".

For pressure-driven flows, this expression can be greatly simplified, and the solution of Pinho and Oliveira (2000)

can be recovered (cf. their Eq. 40—note that a different definition of Br and the opposite convention for $\dot{q}_w$ were used by Pinho and Oliveira 2000). Further simplifications can be obtained when $\sqrt{\varepsilon}\,Wi_N = 0$ (i.e., constant viscosity fluids, either Newtonian or Boger fluids), leading to the following simplified equation (for $Jo = 0$ and $\Gamma^{-1} \to 0$):

$$Nu = \frac{140}{17 + 72\,Br} \tag{37}$$

Additionally, for pure electro-osmosis with high H^+ the velocity profile approaches a plug, and in the absence of viscous dissipation and Joule heating the Nusselt number expression simplifies to $Nu = 12$, as it should.

4 Results and discussion

The solution of forced convection in dynamic and thermally fully developed channel flow of a simplified Phan-Thien–Tanner fluid induced by combined electro-osmosis and pressure gradient forcings was derived in the previous sections for constant wall heat flux and including the effects of viscous dissipation and Joule heating. In this section we analyse the effect of the relevant dimensionless parameters on the velocity, shear stress and temperature profiles, and their influence on the resulting Nusselt number. Even though Afonso et al. (2009) investigated in detail these effects on the velocity profiles, it is worth doing it here because of the different velocity normalization used, which affects significantly the shape of the profiles as well as the understanding of the dynamic and thermal problems.

The discussion starts with the analysis of the variation of the ratio between the bulk and the Helmholtz–Smoluchowski velocities, $\bar{u}/u_{\mathrm{sh}}$, as a function of the relevant dimensionless groups. We note that in Fig. 1 the electric field is assumed positive and $\psi_0 < 0$, leading to a positive Helmholtz–Smoluchowski velocity. When the pressure gradient is favourable it forces flow in the same direction of electro-osmosis, $\Gamma = -3u_N/u_{\mathrm{sh}} < 0$, whereas for an adverse pressure gradient the pressure-induced flow is opposed to the Helmholtz–Smoluchowski velocity and $\Gamma > 0$. The analytical solutions derived in this work are general and allow for any sign in the applied electric field and pressure gradient. Since these two forcing mechanisms appear always combined what really matters is the variation of one relative to the other. Figure 2 shows the variation of $\bar{u}/u_{\mathrm{sh}}$ as a function of $\sqrt{\varepsilon}\,Wi_\kappa$, with the EDL thickness, H^+, and Γ as parameters. The influence of H^+ is analysed considering a relatively low value, $H^+ = 20$ (dashed curves), and another case with a thinner Debye layer, $H^+ = 100$ (solid curves). In the absence of pressure gradient ($\Gamma = 0$) the ratio $\bar{u}/u_{\mathrm{sh}}$ increases with $\sqrt{\varepsilon}\,Wi_\kappa$ on account of the shear-thinning viscosity, which reduces the viscous resistance to motion at the wall. By reducing the thickness of the EDL (higher H^+) the plug of velocity is slightly wider and consequently the flow rate is slightly larger. Adding a favourable pressure gradient ($\Gamma < 0$) further enhances the growth of $\bar{u}/u_{\mathrm{sh}}$, with this effect being stronger with thicker EDLs. This is so because the region of lower shear viscosity (on account of shear-thinning behaviour) is wider for thicker EDLs and this contributes more effectively to enhance the flow rate associated with the pressure contribution than to reducing the corresponding electro-osmosis contribution (the width of the central plug decreases from the thin to the thick EDL), even though the viscosities may not be as low and the Helmholtz–Smoluchowski velocity as high as for the thin EDLs (this also helps reduce the EO flow rate for thick EDL relative to thin EDL).

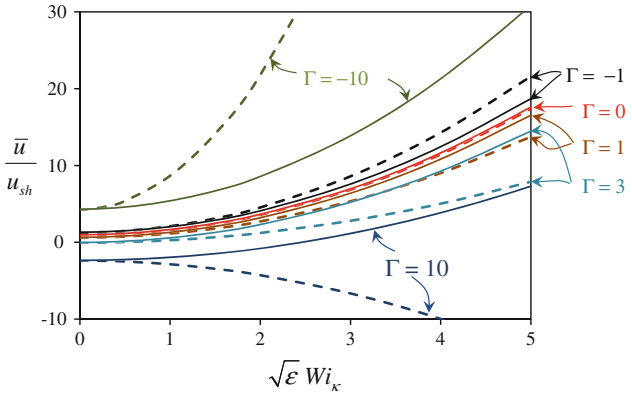

Fig. 2 Dimensionless average velocity as function of $\sqrt{\varepsilon}\,Wi_\kappa$ for various pressure to electro-osmotic forcing ratios, Γ. *Dashed curves* correspond to $H^+ = 20$ and continuous curves to $H^+ = 100$

The most intriguing results in Fig. 2 concern adverse pressure gradient conditions. There is an overall reduction in $\bar{u}/u_{\mathrm{sh}}$ with increasing Γ because pressure-driven flow opposes electro-osmosis (i.e., whatever their shape, all lines for $\Gamma > 0$ are below the line for $\Gamma = 0$). Still for $\Gamma = 1$ electro-osmosis is stronger than pressure flow and the bulk flow remains positive. Further increasing Γ increases pressure-driven flow so much that a reverse bulk velocity sets in. For $H^+ = 100$ and $\Gamma = 10$ the zero bulk flow condition occurs at $\sqrt{\varepsilon}\,Wi_\kappa \approx 2.5$, meaning that the backward flow induced by the adverse pressure gradient equals the forward flow associated with electro-osmosis. For thin EDL the overall viscosity decrease associated with shear-thinning is more localized and it impacts more upon the forward electro-osmosis flow than over the backward pressure-driven flow and so a backward bulk velocity is only observed for low values of $\sqrt{\varepsilon}\,Wi_\kappa$ and we always observe an increase in $\bar{u}/u_{\mathrm{sh}}$ with $\sqrt{\varepsilon}\,Wi_\kappa$. As for favourable pressure gradient, thickening the Debye layer for $\Gamma = 10$ suffices to enhance significantly the reversed flow driven by the adverse pressure gradient to levels exceeding

the enhancement of forward electro-osmosis flow (this variation is relative to a constant viscosity fluid), with the consequence that the flow rate continuously increases in the reverse direction (negative values of $\bar{u}/u_{sh}$). The change of sign in $\bar{u}/u_{sh}$, depending on the dimensionless parameters H^+, Γ and $\sqrt{\varepsilon}\,Wi_\kappa$, will obviously have a strong impact upon the progression of the velocity profiles, as discussed below.

Velocity profiles are presented in Fig. 3 for $\sqrt{\varepsilon}\,Wi_\kappa = 3$. As expected, increasing H^+ leads to higher velocity gradients near the wall, which can have a significant influence on the dimensionless velocity profile, as shown for a strong adverse pressure gradient flow, $\Gamma = 10$ (cf. cases for $\Gamma = 10$ and $H^+ = 20$ and 100, and the previous discussion of Fig. 2). For viscoelastic fluids the velocity profiles are flatter than for Newtonian fluids (not shown), a typical consequence of shear-thinning, and an inversion of the velocity profile is observed for $\Gamma = 10$ and $\sqrt{\varepsilon}\,Wi_\kappa = 3$, as discussed above. In this case the maximum normalized velocity occurs near the wall, and the minimum value is found on the centre of the channel. For $\Gamma = 10$ and $H^+ = 100$ the change of sign in $\bar{u}/u_{sh}$ observed in Fig. 2 at $\sqrt{\varepsilon}\,Wi_\kappa \approx 2.5$ is responsible for the inversion of the dimensionless velocity profile near the walls, as shown in Fig. 3. Also, the large velocity overshoot observed near the wall for $\Gamma = 10$, $H^+ = 100$ and $\sqrt{\varepsilon}\,Wi_\kappa = 3$ occurs due to both the enhanced local EO velocity (the true Helmholtz–Smoluchowski velocity has increased due to the low local value of the shear-thinning viscosity) in addition to the normalization by a low average velocity for these flow conditions (cf. Fig. 2). In fact the integral of the normalized velocity is always 1, by definition, and since the bulk velocity is close to zero, this implies positive and negative values, which are artificially increased with a normalization by a small value.

Figure 4 illustrates the influence of Γ on the transverse profiles of the dimensionless shear stress, τ^+_{xy}, for a sPTT fluid at $\sqrt{\varepsilon}\,Wi_\kappa = 3$, assuming a value of $H^+ = 100$. All the profiles show the strong gradients of shear stress near the wall, induced by the local high shear rates, and a quasi-linear variation elsewhere. For $\Gamma = 10$ we observe a change of sign of τ^+_{xy} near the wall, which is induced by the change of sign of $\bar{u}$ and hence of the normalizing stress $\tau_{w,p}$ (cf. Eq. 24). This parameter is represented in Fig. 5 as function of Γ for a range of $\sqrt{\varepsilon}\,Wi_\kappa$ values, including the limiting case of Newtonian fluid ($\sqrt{\varepsilon}\,Wi_\kappa = 0$). This particular solution includes both the Newtonian case and the sPTT case with $\varepsilon = 0$, i.e., the upper-convected Maxwell (UCM) model solution. For convenience, the $\tau_{w,p}$ parameter is here normalized by the shear stress at the wall for pure Poiseuille flow of a Newtonian fluid flowing at the same average velocity ($\tau_{w,N} = 3\,\eta\,\bar{u}/H$), thus leading to the asymptotic behaviour illustrated in Fig. 5 at large values of $|\,\Gamma\,|$ for Newtonian fluid flow: $\tau_{w,p}/(3\,\eta\,\bar{u}/H) \to 1$. As shown in Fig. 5, $\tau_{w,p}/(3\,\eta\,\bar{u}/H)$ is a positive quantity, therefore the sign of $\tau_{w,p}$ is coincident with the sign of $\bar{u}$. For the Poiseuille flow of a viscoelastic fluid ($\Gamma^{-1} \to 0$), Fig. 5 shows that $\tau_{w,p}/(3\,\eta\,\bar{u}/H)$ decreases continuously when the viscoelastic non-linear behaviour is enhanced (by increasing $\sqrt{\varepsilon}\,Wi_\kappa$), because the shear thinning nature of the sPTT fluid reduces the wall shear stress and enhances the flow rate/bulk velocity ($\bar{u}$). The vertical asymptotes shown in Fig. 5 correspond to flow conditions with a vanishing net flow rate ($\Gamma = \Gamma_0$), or null average velocity, which occur for adverse pressure gradient flow conditions

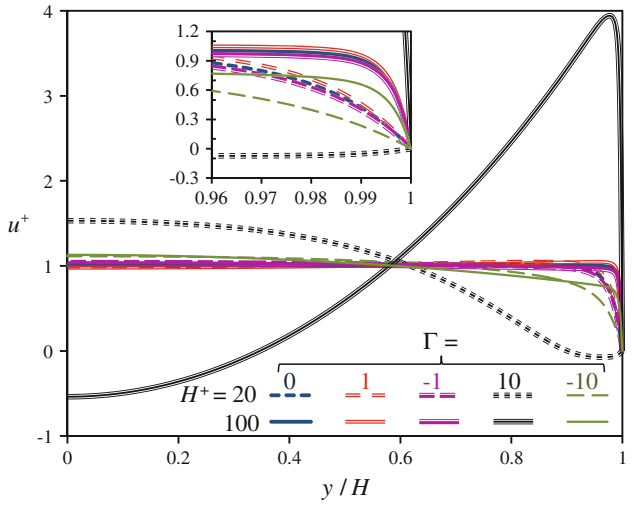

Fig. 3 Dimensionless velocity profiles for viscoelastic fluid flow at $\sqrt{\varepsilon}\,Wi_\kappa = 3$. Influence of the pressure to electro-osmotic forcing ratio Γ and the inverse dimensionless EDL thickness, H^+

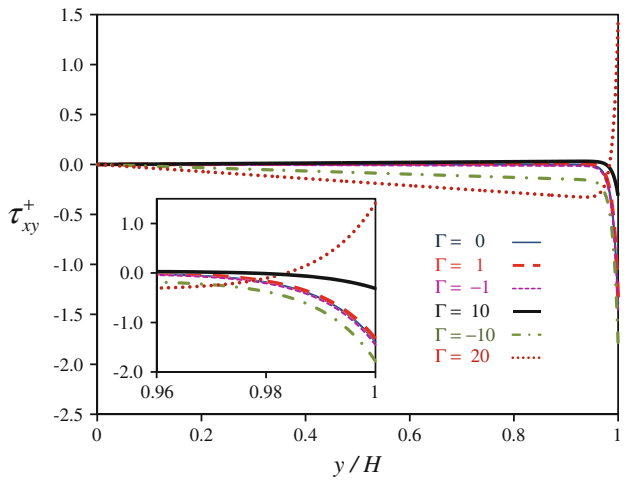

Fig. 4 Transverse profiles of normalized shear stress for viscoelastic fluid flow at $\sqrt{\varepsilon}\,Wi_\kappa = 3$. Influence of the pressure to electro-osmotic forcing ratio, Γ, for $H^+ = 100$

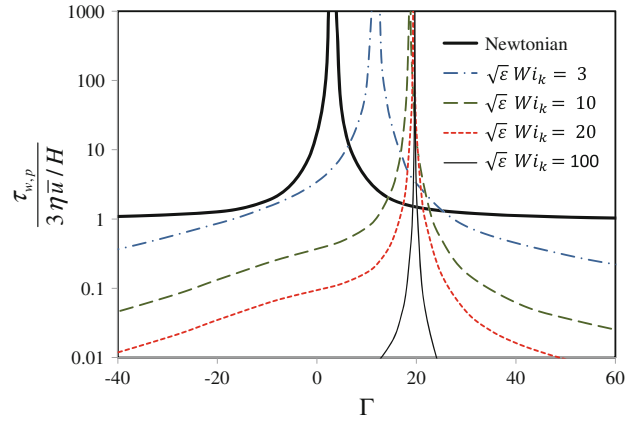

Fig. 5 Variation of the normalized $\tau_{w,p}$ as function of pressure to electro-osmotic forcing ratio, Γ, and generalized Weissenberg number, $\sqrt{\varepsilon}\,Wi_\kappa$, for $H^+ = 100$

at increasingly higher Γ_0 values when $\sqrt{\varepsilon}\,Wi_\kappa$ increases. This condition corresponds to the cases when the flow induced by electro-osmosis is equal in strength, but of opposite sign, to that produced by the adverse pressure gradient.

Figure 6 shows transverse profiles of the dimensionless temperature difference, $T_w^+ - T^+$, for different values of *Jo* and *Br*. All cases correspond to a specific situation with a zero dimensionless axial temperature gradient, which occurs when $Jo + 32Br = -4$ (cf. Eq. 27). Figure 6 considers the limiting cases of pure electro-osmotic flow, and pure pressure-driven flow. In both cases comparison is made between the Newtonian case (right part of the figure)

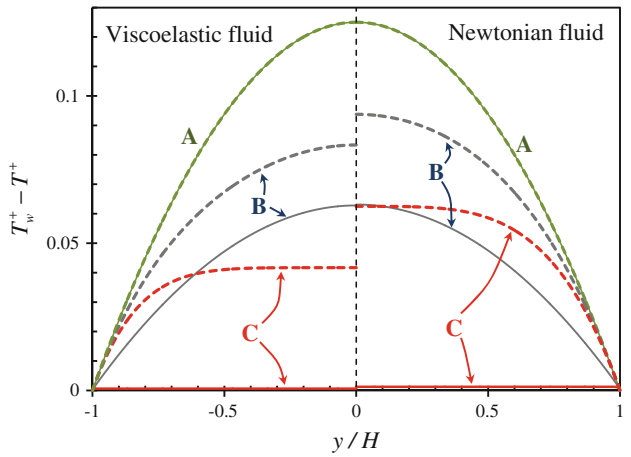

Fig. 6 Transverse profiles of normalized temperature difference when $\partial T^+/\partial x' = 0$ for pure electro-osmosis ($\Gamma = 0$; $H^+ = 100$ *full lines*) and pure Poiseuille flow ($\Gamma^{-1} \to 0$ *dashed lines*). Comparison between Newtonian (positive *y*/*H* axis) and viscoelastic cases (negative *y*/*H* axis $\sqrt{\varepsilon}\,Wi_\kappa = 10$ for $\Gamma = 0$ and $\sqrt{\varepsilon}\,Wi_N = 10$ for $\Gamma^{-1} \to 0$). *A* $Jo = -4$; $Br = 0$; *B* $Jo = -2$; $Br = -0.0625$; *C* $Jo = 0$; $Br = -0.125$

and a viscoelastic case (left part) at a significantly high elasticity level ($\sqrt{\varepsilon}\,Wi_\kappa = 10$ for pure EO and $\sqrt{\varepsilon}\,Wi_N = 10$ for pure Poiseuille flow). When the heat generation is solely due to Joule effect, the temperature profiles coincide for all cases, independently of the viscoelasticity level and the flow mechanism (i.e. for any Γ). This is easily understood from Eq. 14, which for $Br = 0$, $Jo = -4$ and $dT^+/dx' = 0$ leads to the general solution $T_w^+ - T^+ = [1 - (y/H)^2]/8$. The influence of the viscous dissipation is confined to the region with non-negligible shear rate, and for the pure electro-osmotic flow this is particularly enhanced with the temperature variation being limited to the Debye layer region. Shear-thinning of the sPTT model influences the heat generated by viscous dissipation and leads to a reduction of the heat generated. The curves C in Fig. 6 for $\Gamma = 0$ also indicate that viscous dissipation is not very important in electro-osmotic flows with large H^+ values (which are typically observed in microfluidics—the case illustrated in Fig. 6 corresponds to $H^+ = 100$), but for pressure-driven flows or mixed kinematic flows the influence of viscous dissipation is more significant. The curves A and B ($Jo \neq 0$) illustrated in Fig. 6 for pure Poiseuille flow ($\Gamma^{-1} \to 0$) should be regarded as the limiting behaviour at large $|\Gamma|$, because the flow is induced exclusively by a pressure gradient forcing and no electrical field is expected to be applied. This limiting case can also be observed when both a pressure gradient and an electrical field are applied to the system, but the zeta potential is vanishingly small, and no electro-osmotic flow is induced, but Joule heating occurs. This is not a common situation, but serves to test the limiting behaviour of the analytical solution.

Figure 7 plots the transverse profiles of the dimensionless temperature difference for a favourable pressure gradient flow ($\Gamma = -1$), considering wall cooling with $Br = -0.1$ (Fig. 7a, implying negative values for $\dot{q}_w$ and *Jo*) and wall heating with $Br = 0.1$ (Fig. 7b, implying positive values for $\dot{q}_w$ and *Jo*) for a range of *Jo* values. We look first to the right-half part of Fig. 7a, pertaining to Newtonian fluids (or viscoelastic fluids of constant viscosity, such as the UCM model) and $Br = -0.1$. Here, the case $Jo = -0.1$ and $Br = -0.1$ corresponds to a situation where the wall cooling is slightly higher than the internal heat generation, but the normalized temperature gradient is positive ($\partial T^+/\partial x' > 0$), because in spite of a reduction in real temperature ($\partial T/\partial x < 0$) the wall heat flux is negative ($\dot{q}_w < 0$). The other cases, with $Jo \leq -1$ concern high Joule heating leading to an increase in dimensional temperature ($\partial T/\partial x > 0$), but since there is cooling at the wall the non-dimensional temperature gradient ends up as negative ($\partial T^+/\partial x' < 0$). The plotted profiles refer to $T_w^+ - T^+ = (T_w - T)/(\dot{q}_w D_h/k_{th})$, a quantity which also changes sign

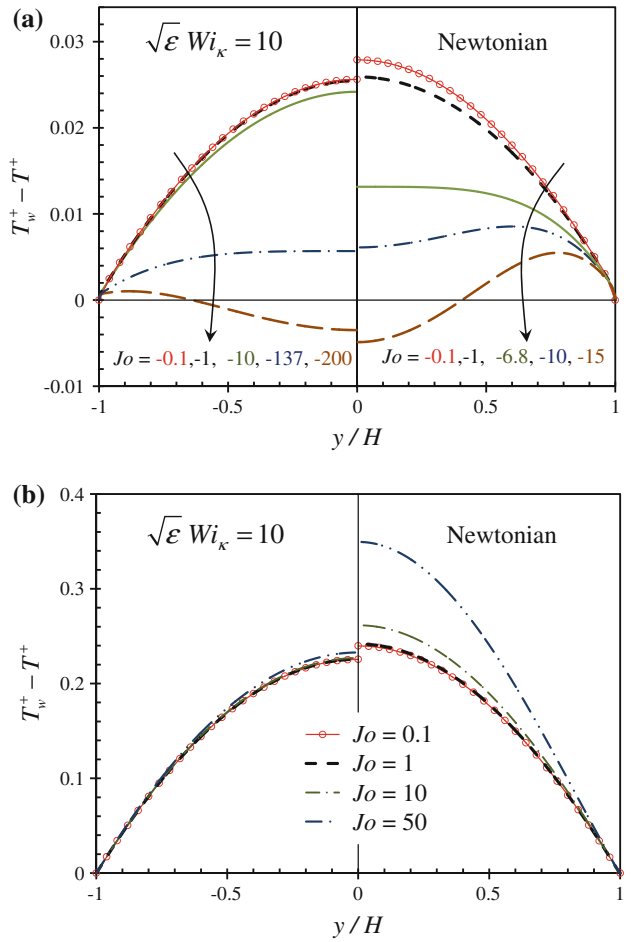

Fig. 7 Transverse profiles of normalized temperature difference for $\Gamma = -1$ and $H^+ = 100$. Comparison between Newtonian (positive y/H axis) and a strong viscoelastic case, $\sqrt{\varepsilon}\,Wi_\kappa = 10$ (negative y/H axis) for a range of Jo values: **a** wall cooling and $Br = -0.1$; **b** wall heating and $Br = 0.1$

with $\dot{q}_w$. For $Jo = -0.1$ and $Jo = -1$, $T > T_w$ everywhere across the channel, but $(T_w^+ - T^+)$ ends up as a positive quantity because of the negative $\dot{q}_w$. The dimensional temperature T continuously decreases from the axis towards the wall and the concavity of the dimensionless profile is the same everywhere. However, on increasing the Joule heating to $Jo = -10$ (in absolute terms), the internal heat generation exceeds by far the amount of heat removed at the wall and not only the dimensional temperature increases in the stream-wise direction, as pointed out above, but the fluid at around $0.5 < y/H < 0.7$ cools to the wall as well as towards the centre, i.e., instead of the single peak value of $(T_w^+ - T^+)$ at the centre line there is a positive peak in the vicinity of $y/H \approx +0.6$ (and at $y/H \approx -0.6$ by symmetry) and a local minimum at the centreline, which even becomes negative at higher Joule heating conditions, as displayed in Fig. 7a for $Jo = -15$. This change in the dimensionless temperature difference profile is synonymous to the onset of a change of concavity of temperature on the channel symmetry axis ($y = 0$), and the critical value of Jo at which this occurs is given by $Jo_{cr} = u^+|_{y^+=0}(\partial T^+/\partial x')$ as easily deduced from Eq. 14. Using Eq. 27 one ends up with the following expression: $Jo_{cr} = (4 + 32Br)\,u^+(0)\,/(1 - u^+(0))$. For a Newtonian fluid at $\Gamma = -1$ and $H^+ = 100$ the centreline velocity is $u^+(0) = 1.1335$, therefore for $Br = -0.1$ we obtain $Jo_{cr} = -6.8$, and the corresponding temperature profile is also included in Fig. 7a. For the viscoelastic case, at $\Gamma = -1$, $H^+ = 100$ and $\sqrt{\varepsilon}\,Wi_\kappa = 10$ the centreline velocity is $u^+(0) = 1.00587$ and $Jo_{cr} = -137$ for $Br = -0.1$, showing that the influence of Jo on the temperature profile is much less significant as shown in Fig. 7a (there would be no such influence for a constant velocity profile). As the internal heat generation further increases above Jo_{cr} the bulk temperature will eventually become lower than the wall temperature, i.e., the positive Nu goes to infinity and changes sign, as shown later.

For positive values of Br and Jo (illustrated in Fig. 7b) the fluid is being heated at the wall ($\dot{q}_w > 0$) and $T_w > T$, so we have again $(T_w^+ - T^+) > 0$. In addition to the wall heating, the fluid heats also internally by viscous dissipation and Joule heating effects, hence it is no surprise that the temperatures differences $(T_w^+ - T^+)$ inside the fluid are now larger than for negative values of Br and Jo. The Joule heating is essentially uniform across the channel and independent of the velocity profile shape so it affects the magnitude of the temperature, but not the shape of $(T_w^+ - T^+)$. If the Brinkman number was higher the shape would also be similar, because wall heating forces $T_w > T$ near the wall and viscous dissipation acts more intensively near the wall. Here, it raises the temperature (T) locally, while keeping $T_w > T$. This effect is transmitted across the duct as heat flows towards the centre and heats the fluid (note that at the centre itself the heat flux is null). Thus, this mechanism maintains the shape of $(T_w^+ - T^+)$, but with a different magnitude for different internal heating.

Changing from a Newtonian fluid to a strong shear-thinning fluid characterized by $\sqrt{\varepsilon}\,Wi_\kappa = 10$ there is a reduction of the viscosity in the wall region, typical of shear-thinning behaviour. Then, we see the mean velocity increases significantly due both to the EO contribution (when the wall viscosity decreases the true Helmholtz–Smoluchowski velocity increases, cf. Afonso et al. 2009) as well as by the pressure contribution as hinted in Fig. 2 (although $\sqrt{\varepsilon}\,Wi_\kappa = 10$ is outside the range in this plot, the corresponding line for $\Gamma = -1$ and $H^+ = 100$ indicates that the ratio $\bar{u}/u_{sh}$ is now very large). Additionally, and this is the most important reason to explain the slight decrease in the sPTT profiles of $T_w^+ - T^+$ for $\sqrt{\varepsilon}\,Wi_\kappa = 10$

relative to the corresponding Newtonian profiles in Fig. 7, by reducing the wall viscosity the velocity profile becomes flatter, i.e., the distribution of the total flow rate across the channel is changed and there is now more flow near the wall and a concomitant decrease of flow away from the wall than for the Newtonian flows. Since the proportion of fluid flowing close to the wall increases with $\sqrt{\varepsilon}\,Wi_\kappa$, shear-thinning reduces the thermal resistance, hence it increases the heat transfer coefficient (Nusselt number) and the temperature differences can be lower for the same wall heat flux. This also makes the shear-thinning profiles less sensitive to the variation of Jo (as mentioned above complete insensitivity, $Jo_{cr} \to \infty$, comes for a plug velocity profile).

The Nusselt number is also an important parameter that was quantified in the theoretical analysis of the previous section, and Figs. 8, 9, 10 illustrate how Nu is influenced by the relevant parameters, namely Γ, $\sqrt{\varepsilon}\,Wi_\kappa$ (or $\sqrt{\varepsilon}\,Wi_N$ for pressure-driven flow), Jo and Br. In all cases analysed with electro-osmosis $H^+ = 100$ was used, but this parameter also influences the Nusselt number, except for pure pressure-driven flow.

Figure 8 illustrates the influence of Br and Jo on the Nusselt number of Newtonian and viscoelastic fluid flow for the situation where $\partial T^+/\partial x' = 0$, a particular case of wall cooling. Pure electro-osmosis ($\Gamma = 0$), pure Poiseuille flow ($\Gamma^{-1} \to 0$) and weak favourable and adverse pressure gradient flow conditions ($\Gamma = -1$ and 1, respectively) are considered, assuming a constant axial temperature profile, $\partial T^+/\partial x' = 0$, which implies the relation $Jo + 32Br = -4$, as already discussed. The results show that the minimum Nu values are observed for pure Poiseuille flow, and large Nu values are observed when viscous dissipation

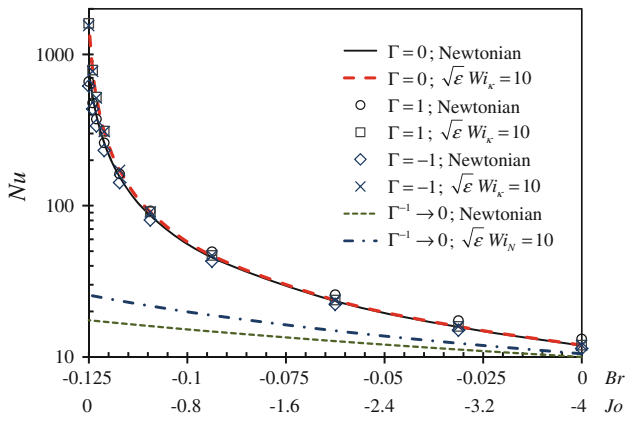

Fig. 8 Variation of Nusselt number with Br and Jo for constant axial temperature (wall cooling), $dT^+/dx' = 0$ (cf. Eq. 27) for several values of Γ and $H^+ = 100$ considering a Newtonian and a viscoelastic fluid

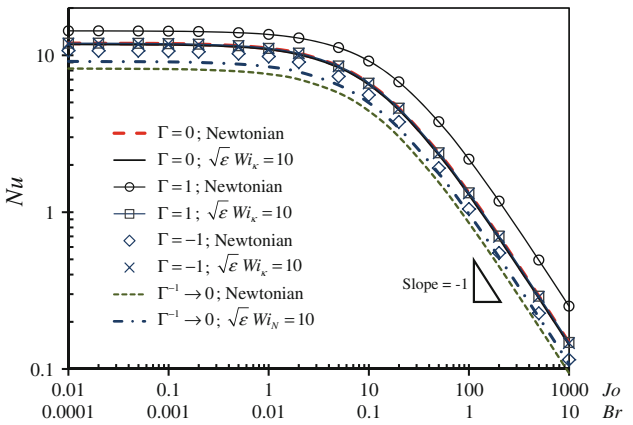

Fig. 9 Variation of Nusselt number with Br and Jo, assuming that $Br = Jo/100$ and wall heating conditions. $H^+ = 100$ was assumed for $\Gamma = 0$ and $\Gamma = \pm 1$ cases. Comparison between Newtonian and viscoelastic fluids

increases (large $|Br|$). Viscous dissipation is stronger near the wall, so larger values of Br are synonymous to situations where the amount of heat to be removed at the wall comes in a higher proportion from fluid closer to the wall than from the centre. This is equivalent to a lower thermal resistance and hence higher Nu. Since normalization implies the same cooling at the wall, wall temperature gradients will be essentially the same, but with less heat coming proportionally from the centre of the channel the temperature difference $(T_w^+ - \bar{T}^+)$ is reduced. This is consistent with the temperature profiles shown in Fig. 6 and the relationship between Nu and $(T_w^+ - \bar{T}^+)$ in Eq. 34.

For pure electro-osmosis, $\Gamma \to 0$, with very large H^+, negligible viscous dissipation and $\partial T^+/\partial x' = 0$ (i.e. $Jo = -4$), the asymptotic value of $Nu = 12$ is approached as shown next, the classical solution for plug flow (Burmeister 1983) (actually, in the absence of viscous dissipation and for a plug flow velocity profile $Nu = 12$ regardless of $\partial T^+/\partial x'$). In this limiting case the velocity profile $u(y) \approx \bar{u}$ (except within the Debye layer, which reduces in width as H^+ increases), or $u^+ \approx 1$ and the energy Eq. 14 simplifies to $d^2T^+/dy^{+2} + Jo/(16H^{+2}) = 0$ with $Jo = -4$, which can be integrated twice to give the temperature profile $T_w^+ - T^+ = \left[1 - (y^+/H^+)^2\right]/8$. Using Eq. 35 the average temperature difference is $T_w^+ - \bar{T}^+ = 1/12$, and consequently $Nu = 1/(T_w^+ - \bar{T}^+) = 12$. The corresponding $\partial T^+/\partial x' = 0$ Newtonian solution for pressure-driven flow ($\Gamma^{-1} \to 0$) and no Joule heating has $Jo = 0$ and $Br = -0.125$, leading to $Nu = 17.5$ as easily calculated using Eq. 37 and observed in Fig. 8.

Figure 9 illustrates the influence of Jo on the Nusselt number for Newtonian and viscoelastic fluid flow with

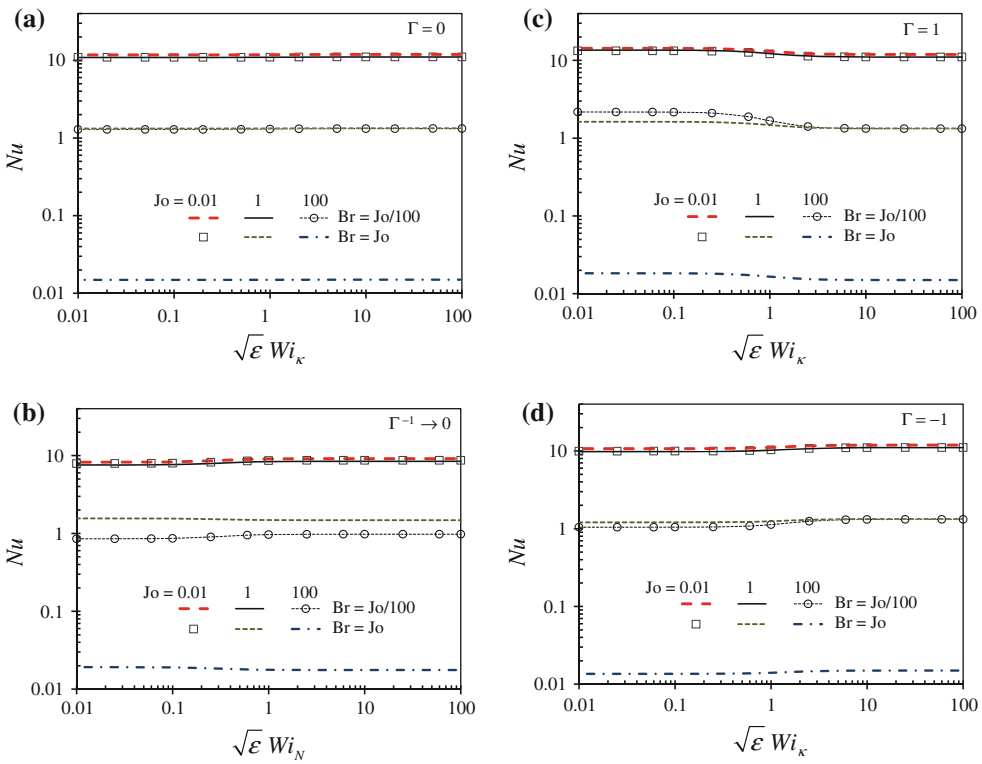

Fig. 10 Influence of the elasticity on the Nusselt number for a range of *Br* and *Jo* parameters, considering wall heating conditions. **a** Pure electro-osmosis ($\Gamma = 0$ and $H^+ = 100$); **b** Poiseuille flow; **c**, **d** mixed driving forces with adverse and favourable pressure gradients ($\Gamma = 1$ and -1, respectively), assuming $H^+ = 100$

wall heating. Again, pure electro-osmosis ($\Gamma = 0$), pure Poiseuille flow ($\Gamma^{-1} \to 0$) and weak favourable and adverse pressure gradient flow conditions ($\Gamma = -1$ and 1, respectively) are considered, assuming that $Br = Jo/100$. The simultaneous variation of *Br* and *Jo* can be achieved experimentally by varying the heat flux transferred through the wall, and a significantly larger *Jo* was assumed ($Jo = 100Br$), as expected for microfluidic applications. Indeed, as discussed by Maynes and Webb (2004), viscous heating will contribute significantly to the total temperature rise of the fluid, and consequently to changes in *Nu*, only in nanoscale channels, where H^+ is typically small, a condition not considered here due to the use of the Debye–Hückel approximation. The results show that increasing the internal heat generation relative to wall heating (i.e. increasing *Jo* and *Br*) also leads to a reduction of the Nusselt number, particularly at high *Jo* (and *Br*) values, where *Nu* is found to be inversely proportional to *Jo*. This is so because as internal heating increases, the fluid bulk temperature increases, the temperature difference $(T_w^+ - \bar{T}^+)$ also increases and by so much that for the same wall heat flux the convection coefficient (and *Nu*) is progressively reduced. Actually, for high values of *Jo* (and *Br*) the fluid heats significantly more by the internal heating than by the wall heating, so that $(T_w^+ - \bar{T}^+) \to \infty$ as *Jo* (and *Br*) increase and correspondingly $Nu \to 0$, cf. Eq. 34. This is consistent with the temperature profiles shown in Fig. 7b and the corresponding discussion.

Finally, in Fig. 10 we show the influence of fluid rheology on the Nusselt number for pure electro-osmosis ($\Gamma = 0$), Poiseuille flow ($\Gamma^{-1} \to 0$) and weak favourable and adverse pressure gradient flow conditions ($\Gamma = \pm 1$) using a range of *Jo* values and assuming either that $Br = Jo/100$ or $Br = Jo$ (wall heating). This latter situation is less probable in microfluidic applications, but allows to better highlight the influence of *Br* on *Nu*. In all cases the influence of viscoelasticity is not very important, and increasing either *Jo* or *Br* leads to a reduction of *Nu*, in agreement with the results displayed in Fig. 9 and the explanation given to explain such variations.

To finalize, and for the purpose of benchmarking we provide in Table 1 a set of Nusselt number values under various conditions. The negative Nusselt numbers correspond to very intense internal heating for wall cooling as discussed in regard to Fig. 7a. Negative Nusselt numbers are not uncommon in the literature (e.g. Vick and Özisik 1981; Ong and Owen 1991) and tend to occur in specific situations, such as when there is a strong internal heat generation that reverses the magnitude of the temperature difference used in the definition of the heat transfer coefficient (here Eq. 34), but the local wall heat flux sign remains unchanged.

Table 1 Influence of the relevant dimensionless parameters on the Nusselt number ($H^+ = 100$; $Br = Jo/100$)

$\sqrt{\varepsilon}\,Wi_\kappa$	$\Gamma = 10$			$\Gamma = -10$		
	$Jo = 0$	$Jo = 10$	$Jo = -10$	$Jo = 0$	$Jo = 10$	$Jo = -10$
0	7.169	3.249	-34.770	8.905	4.411	−472.853
1	6.521	2.759	-17.951	9.390	4.664	−695.361
10	12.757	7.472	43.592	11.644	6.374	67.294

Note that $Jo > 0$ corresponds to wall heating and $Jo < 0$ to wall cooling conditions

5 Conclusions

The analytical solutions for flow and heat transfer in a fully developed channel flow of a simplified Phan-Thien–Tanner fluid forced by combined electro-osmosis and pressure gradient are presented and discussed. This solution invokes the standard electrokinetic conditions and the Debye–Hückel approximation. Even though the flow solution was previously obtained by Afonso et al. (2009), the present solution uses the bulk velocity, rather than the Helmholtz–Smoluchowski velocity, as a velocity scale thus allowing for a more compact expression. As a consequence of the different normalization used here there are some conceptual differences in the fluid dynamical solution relative to Afonso et al. (2009).

For the forced convection solution a constant wall heat flux is imposed and it is assumed that temperature differences are sufficiently small for the model parameters to be independent of temperature. In addition to the dependence on the non-dimensional numbers controlling the flow solution, i.e., on the normalized electric double layer (EDL) thickness, Weissenberg number and Γ, the ratio between the electro-osmotic and pressure gradient forcings, the thermal solution includes the effects of viscous dissipation and of Joule heating by the electric current. These two effects are quantified in the non-dimensional Brinkman and Joule numbers, respectively.

For pure electro-osmosis and thin EDL viscous dissipation is concentrated at the near-wall region and its effect is negligible by comparison with Joule heating which is whole-field and hence more relevant. When there is equilibrium between internal heating and wall cooling ($\partial T^+/\partial x' = 0$) and the former is solely by Joule effect the invoked decoupling of the material properties and temperature implies the thermal solution is independent of the amount of viscoelasticity and type of flow (Γ) since Joule heating does not depend on the specific form of the velocity profile in contrast to viscous dissipation, which is proportional to the shear rate. For this reason, viscous dissipation is restricted to the near-wall region in pure electro-osmosis flow, so it is essentially irrelevant for very thin electric double layers. However, for $\partial T^+/\partial x' \neq 0$ the effects of Joule and Brinkman heating are coupled with any cause of variation in the bulk flow velocity, and hence of u^+, as is obvious from inspection of Eq. 14. As the EDL thickens and/or the pressure gradient contribution increases the region affected by viscous dissipation grows and non-linear rheological effects, such as shear-thinning viscosity, appear more clearly to affect all dynamic and thermal quantities. In practical terms for viscous dissipation to become very important requires very small channels (nano-channels), but then the Debye–Hückel approximation ceases to be valid. Alternatively the fluid viscosity and/or flow rate must be increased, but then the pressure losses become so large that the channels might suffer structural damage. As known from Pinho and Oliveira (2000) in the absence of viscous dissipation enhancing shear-thinning for pure Poiseuille flow increases Nu, whereas for pure electro-osmosis it decreases Nu by a small amount. For wall heating, increasing levels of internal heat generation, by whatever mechanism, is seen to increase significantly the temperature differences within the fluid and consequently to reduce the corresponding Nusselt numbers, whereas for wall cooling there is a reduction in temperature differences within the fluid as internal heat generation increases.

Acknowledgments The authors wish to thank funding by Fundação para a Ciência e a Tecnologia and FEDER through projects PTDC/EQU-FTT/70727/2006, PTDC/EQU-FTT/71800/2006 and PTDC/EQU-FTT/113811/2009. M.A. Alves also acknowledges the Department of Chemical Engineering of FEUP for conceding a sabbatical leave.

Appendix

For the sake of conciseness of the main body of the paper, this appendix presents the mathematical expressions for the coefficients appearing in Eqs. 29 and 36.

The normalized temperature gradient of Eq. 29 is a function of the following coefficients:

$$\theta_1 = -\frac{\delta_1 z_1 Br}{4H^+};\ \theta_2 = \frac{Br}{3H^+}(2\delta_2 z_1 + \delta_1 z_2);$$
$$\theta_3 = \frac{1}{144 H^{+2}}\left[16 Br H^+(2\delta_2 z_1 + \delta_1 z_2) + 3\omega_1 \frac{\partial T^+}{\partial x'}\right];$$
$$\theta_4 = \frac{Br}{2H^+}(z_4\delta_1 - 2\delta_2 z_2);$$
$$\theta_5 = \frac{1}{16 H^{+2}} \times \left\{4 Br H^+[(2z_1 + 2z_3 + z_4)\delta_1 - 2\delta_2 z_2] - \omega_2 \frac{\partial T^+}{\partial x'}\right\}$$
$$\theta_6 = \frac{1}{16 H^{+2}}\left[8(2\delta_2 z_2 - \delta_1 z_4) Br H^+ + \omega_2 \frac{\partial T^+}{\partial x'}\right];$$
$$\theta_7 = \frac{2Br}{H^+}(\delta_1 z_5 + \delta_2 z_4);$$
$$\theta_8 = \frac{1}{4H^{+2}}\left\{4 Br H^+\left[(z_2 + 12 z_5 + 2 z_6)\delta_1 + (2z_3 + 12 z_4)\delta_2\right] - \omega_3 \frac{\partial T^+}{\partial x'}\right\};$$
$$\theta_9 = \frac{1}{16 H^{+2}}\left[96 Br H^+(\delta_2 z_4 + \delta_1 z_5) - \omega_3 \frac{\partial T^+}{\partial x'}\right];$$
$$\theta_{10} = \frac{1}{16 H^{+2}}\left\{16 Br H^+\left[(z_2 + 12 z_5 + 2 z_6)\delta_1 + (2z_3 + 12 z_4)\delta_2\right] + (\omega_4 - 4\omega_3)\frac{\partial T^+}{\partial x'}\right\};$$
$$\theta_{11} = -\frac{1}{80 H^{+2}}\left[32 Br H^+ \delta_2 z_5 + \omega_6 \frac{\partial T^+}{\partial x'}\right];$$
$$\theta_{12} = \frac{1}{48 H^{+2}}\left[16 Br H^+(\delta_1 z_4 - 2\delta_2 z_6) + \omega_5 \frac{\partial T^+}{\partial x'}\right]$$
$$\theta_{13} = \frac{1}{16 H^{+2}}\left[16 Br H^+ \delta_1 z_3 - \omega_7 \frac{\partial T^+}{\partial x'} + Jo\right] \qquad (38)$$

and

$$\delta_1 = -\frac{\eta u_{sh}\kappa}{\tau_{w,p}}\frac{1}{\cosh(H^+)};\ \delta_2 = \frac{\eta u_{sh}\kappa}{\tau_{w,p}}\frac{\Gamma}{H^{+2}}. \qquad (39)$$

The normalized temperature difference of Eq. 36 is a function of the following coefficients:

$$\Omega_1 = -\frac{\theta_1\omega_1}{56H^+};\ \Omega_2 = \frac{2\theta_2\omega_1 - 3\theta_1\omega_2}{72};$$
$$\Omega_3 = \frac{6\theta_1\omega_2 - \omega_1(\theta_2 + 18\Upsilon_1)}{216 H^+}$$
$$\Omega_4 = \frac{3\theta_1\omega_3 - 3\theta_2\omega_2 + \theta_4\omega_1 - 10\Upsilon_1\omega_2 - 5\Upsilon_3\omega_1}{50}$$
$$\Omega_5 = \frac{1}{3000 H^+}\left[-25 H^{+2}(3\theta_1\omega_3 - 8\theta_2\omega_2 + 6\theta_4\omega_1) + 3\theta_1(25\omega_4 - 12\omega_3) + 36\theta_2\omega_2 - 12\theta_4\omega_1 + 420\Upsilon_1\omega_2 - 300\Upsilon_2\omega_1 + 60\Upsilon_3\omega_1\right]$$
$$\Omega_6 = \Big[8H^{+2}(3\theta_1\omega_6 + 2\theta_2\omega_3 - 6\theta_4\omega_2 - 6\theta_7\omega_1) - 3\theta_1(4\omega_5 - 3\omega_6 - 32) + 2\theta_2(11\omega_3 - 8\omega_4) - 30\theta_4\omega_2 - 18\theta_7\omega_1 + 120\Upsilon_1\omega_3 + 96\omega_2(\Upsilon_3 - \Upsilon_2) - 24\omega_1(\Upsilon_4 + 2\Upsilon_6)\Big]/384$$
$$\Omega_7 = -\Big\{H^{+4}(96\theta_1\omega_6) + 8H^{+2}[3\theta_1(3\omega_6 - 4\omega_5) + 22\theta_2\omega_3 - 30\theta_4\omega_2 - 18\theta_7\omega_1 + 24(\Upsilon_1\omega_3 + 2\Upsilon_3\omega_2 - \Upsilon_4\omega_1)] + 3\theta_1(32\omega_7 - 4\omega_5 + 3\omega_6) + 2\theta_2(11\omega_3 - 8\omega_4) - 30\theta_4\omega_2 - 18\theta_7\omega_1 - 24\omega_1(\Upsilon_4 + 8\Upsilon_5 + 2\Upsilon_6) + 96\omega_2(\Upsilon_3 - 3\Upsilon_2) + 24\Upsilon_1(5\omega_3 - 8\omega_4)\}/(1536H^+)$$
$$\Omega_8 = \frac{H^{+4}(\theta_2\omega_6 - \theta_{11}\omega_1)}{9} - \frac{H^{+2}}{162}[2\omega_1(20\theta_{11} + 9\theta_{12}) + 2\theta_2(9\omega_5 - 20\omega_6) - 9(5\theta_4\omega_3 + 11\theta_7\omega_2 + 8\Upsilon_1\omega_6 - 3\Upsilon_3\omega_3 + 6\Upsilon_4\omega_2)] - \frac{1}{486}\{27\theta_1\omega_3 + 18\omega_1(2\theta_{12} + 3\theta_{13}) - 2\theta_2(27\omega_7 - 18\omega_5 + 40\omega_6) + 9\theta_4(3\omega_4 - 10\omega_3) - 198\theta_7\omega_2 + 80\theta_{11}\omega_1 + 18\Upsilon_1(6\omega_5 - 8\omega_6 - 27) - 27[8\Upsilon_2\omega_3 + 3\Upsilon_3(\omega_4 - 2\omega_3) + \omega_2(6\Upsilon_4 + 6\Upsilon_5 + 7\Upsilon_6)]\}$$
$$\Omega_9 = \frac{H^{+5}(\theta_{11}\omega_1)}{18} + \frac{H^{+3}}{108}\{\omega_1(20\theta_{11} + 9\theta_{12}) - 20\theta_2\omega_6 - 9[\theta_4\omega_3 + 4(\theta_7\omega_2 + \omega_6\Upsilon_1)]\} + \frac{H^+}{648}\{4\omega_1(40\theta_{11} + 18\theta_{12} + 27\theta_{13}) + 8\theta_2(9\omega_5 - 20\omega_6 - 27) - 27\theta_1\omega_3 - 18[\theta_4(10\omega_3 - 3\omega_4) + 22\theta_7\omega_2 + 4\Upsilon_1(4\omega_6 - 3\omega_5) + 6\omega_3(\Upsilon_2 - 3\Upsilon_3) + 6\omega_2(3\Upsilon_4 + 2\Upsilon_6)]\} + \frac{1}{5832H^+}\{27\theta_1(4\omega_3 + 9\omega_4) + 4[2\omega_1(40\theta_{11} + 18\theta_{12} + 27\theta_{13}) + 2\theta_2(18\omega_5 - 40\omega_6 - 27\omega_7) - 9\{\theta_4(10\omega_3 - 3\omega_4) + 22\theta_7\omega_2 + 2\Upsilon_1(27\omega_7 - 6\omega_5 + 8\omega_6) + 3[\Upsilon_2(8\omega_3 - 9\omega_4) + 3\Upsilon_3(\omega_4 - 2\omega_3) + \omega_2(6\Upsilon_4 + 15\Upsilon_5 + 7\Upsilon_6)]\}]\}$$

$$\begin{aligned}\Omega_{10} = {} & \frac{H^{+^6}(\theta_{11}\omega_2)}{6} \\ & + \frac{H^{+^4}}{4}[\omega_2(8\theta_{11}+\theta_{12}) + \omega_6(3\theta_4 - 2\Upsilon_3) - \theta_7\omega_3] \\ & + \frac{H^{+^2}}{12}\{6\omega_2(20\theta_{11}+3\theta_{12}+\theta_{13}) + \theta_2\omega_3 \\ & -3[\theta_4(2\omega_5 - 15\omega_6 - 2) - \theta_7(\omega_1 - 9\omega_3 + \omega_4) \\ & - 4\Upsilon_2\omega_6 + 2\Upsilon_3(5\omega_6 - \omega_5) + \omega_3(4\Upsilon_4 + \Upsilon_6)]\} \\ & + \frac{1}{24}\{3\omega_2(\theta_1 + 120\theta_{11} + 18\theta_{12} + 8\theta_{13}) \\ & - \theta_2(\omega_3 + 2\omega_4) + 3[\theta_4(2\omega_7 - 6\omega_5 + 45\omega_6) \\ & +3\theta_7(\omega_1 - 9\omega_3 + \omega_4) - 2\omega_3(\Upsilon_1 + 3\Upsilon_5) \\ & - 4\Upsilon_2(\omega_5 - 3\omega_6 - 2) + 2\Upsilon_3(3\omega_5 - 15\omega_6 - 2\omega_7) \\ & -2\Upsilon_4(\omega_1 + 6\omega_3 - \omega_4) + \Upsilon_6(2\omega_1 - 7\omega_3 + 2\omega_4)]\}\end{aligned}$$

$$\begin{aligned}\Omega_{11} = {} & -\frac{H^{+^5}}{12}(8\theta_{11}\omega_2 + 3\theta_4\omega_6) \\ & - \frac{H^{+^3}}{8}\{2\omega_2(20\theta_{11}+3\theta_{12}) + \theta_4(15\omega_6 - 2\omega_5) \\ & -9\theta_7\omega_3 + 2[\omega_6(2\Upsilon_2 - 5\Upsilon_3) - \Upsilon_4\omega_3]\} \\ & - \frac{H^{+}}{24}\{6\omega_2(60\theta_{11}+9\theta_{12}+4\theta_{13}) \\ & - \omega_3(\theta_2 + 21\Upsilon_6) + 3[\theta_4(2\omega_7 - 6\omega_5 + 45\omega_6) \\ & + 3\theta_7(\omega_1 - 9\omega_3 + \omega_4) + 2\omega_3(\Upsilon_1 - \Upsilon_5) \\ & + 4\Upsilon_2(3\omega_6 - \omega_5) + 2\Upsilon_3(3\omega_5 - 15\omega_6 - 4) \\ & -2\Upsilon_4(\omega_1 + 6\omega_3 - \omega_4)]\} \\ & - \frac{1}{48H^{+}}\{6\omega_2(60\theta_{11}+9\theta_{12}+4\theta_{13}) \\ & -\theta_2(\omega_3 + 2\omega_4) + 3[\theta_4(2\omega_7 - 6\omega_5 + 45\omega_6) \\ & +3\theta_7(\omega_1 - 9\omega_3 + \omega_4) - 2\Upsilon_1(\omega_3 + 2\omega_4) \\ & +4\Upsilon_2(2\omega_7 + 3\omega_6 - \omega_5) + 2\Upsilon_3(3\omega_5 - 15\omega_6 - 2\omega_7) \\ & - 2\Upsilon_4(\omega_1 + 6\omega_3 - \omega_4) - 2\Upsilon_5(2\omega_1 + 3\omega_3 - 2\omega_4) \\ & +\Upsilon_6(2\omega_1 - 7\omega_3 + 2\omega_4)]\}\end{aligned}$$

$$\begin{aligned}\Omega_{12} = {} & -\frac{H^{+^6}}{3}(5\theta_{11}\omega_3 + 3\theta_7\omega_6) \\ & - H^{+4}[\theta_{11}(70\omega_3 - \omega_4) + 2\theta_{12}\omega_3 + \theta_7(42\omega_6 - \omega_5) \\ & +\omega_6(6\Upsilon_4 + \Upsilon_6)] - \frac{H^{+^2}}{2}\{40\theta_{11}(70\omega_3 - \omega_4) \\ & + 2\theta_{12}(40\omega_3 - \omega_4) + \omega_3(6\theta_{13} - \theta_4 + \Upsilon_3) \\ & -2\Upsilon_4(\omega_2 + 4\omega_5 - 120\omega_6 - 1) \\ & + \theta_7[2\omega_7 + 9\omega_2 - 40(\omega_5 - 42\omega_6)] + 8\Upsilon_5\omega_6 \\ & +2\Upsilon_6(20\omega_6 - \omega_5)\} - \frac{1}{2}\{240\theta_{11}(70\omega_3 - \omega_4) \\ & + 12\theta_{12}(40\omega_3 - \omega_4) + 2\theta_{13}(18\omega_3 - \omega_4) \\ & - \omega_2(\theta_2 + 2\Upsilon_1) - \theta_4(\omega_1 + 6\omega_3 - \omega_4) \\ & + 6\theta_7[2\omega_7 + 9\omega_2 - 40(\omega_5 - 42\omega_6)] \\ & - \Upsilon_3(\omega_1 - 2\omega_3 + \omega_4) \\ & + 2\Upsilon_4[2\omega_7 - 7\omega_2 - 24(\omega_5 - 30\omega_6)] \\ & - 2\Upsilon_5(\omega_2 + 2\omega_5 - 24\omega_6 - 1) \\ & +\Upsilon_6[2\omega_7 + 5\omega_2 - 12(\omega_5 - 20\omega_6)]\}\end{aligned}$$

$$\begin{aligned}\Omega_{13} = {} & \frac{H^{+^7}(\theta_{11}\omega_3)}{6} + \frac{H^{+^5}}{12}[2\theta_{11}(70\omega_3 - \omega_4) + 3\theta_{12}\omega_3 \\ & +12\omega_6(7\theta_7 + \Upsilon_4)] + \frac{H^{+^3}}{4}\{20\theta_{11}(70\omega_3 - \omega_4) \\ & +\theta_{12}(40\omega_3 - \omega_4) + \omega_3(2\theta_{13} - \theta_4) \\ & + 4[\theta_7(\omega_2 - 5\omega_5 + 210\omega_6 + 1) + \Upsilon_4(30\omega_6 - \omega_5) \\ & +\omega_6(\Upsilon_5 + 5\Upsilon_6)]\} + \frac{H^{+}}{12}\{720\theta_{11}(70\omega_3 - \omega_4) \\ & + 36\theta_{12}(40\omega_3 - \omega_4) - 4\theta_2\omega_2 + 6\theta_{13}(18\omega_3 - \omega_4) \\ & - 3[\theta_4(\omega_1 + 6\omega_3 - \omega_4) \\ & -2\{3\theta_7[2\omega_7 + 9\omega_2 - 40(\omega_5 - 42\omega_6)] \\ & +\omega_3(\Upsilon_3 - \Upsilon_2) + \Upsilon_4[2\omega_7 - 7\omega_2 - 24(\omega_5 - 30\omega_6)] \\ & +2\Upsilon_5(12\omega_6 - \omega_5) + 2\Upsilon_6(\omega_2 - 3\omega_5 + 60\omega_6 + 1)\}]\} \\ & + \frac{1}{8H^{+}}[4\{240\theta_{11}(70\omega_3 - \omega_4) + 12\theta_{12}(40\omega_3 - \omega_4) \\ & + 2\theta_{13}(18\omega_3 - \omega_4) - \theta_2\omega_2 - \theta_4(\omega_1 + 6\omega_3 - \omega_4) \\ & + 6\theta_7[2\omega_7 + 9\omega_2 - 40(\omega_5 - 42\omega_6)] \\ & - \Upsilon_1\omega_2 + \Upsilon_2(\omega_4 - \omega_1) - \Upsilon_3(\omega_1 - 2\omega_3 + \omega_4) \\ & + 2\Upsilon_4[2\omega_7 - 7\omega_2 - 24(\omega_5 - 30\omega_6)] \\ & + \Upsilon_5[2\omega_7 - 3\omega_2 - 4(\omega_5 - 12\omega_6)] \\ & +\Upsilon_6[2\omega_7 + 5\omega_2 - 12(\omega_5 - 20\omega_6)]\} - \theta_1\omega_1]\end{aligned}$$

$$\begin{aligned}\Omega_{14} = {} & \frac{H^{+^{10}}(\theta_{11}\omega_6)}{66} + \frac{H^{+^8}}{108}(3\theta_{12}\omega_6 - 2\theta_{11}\omega_5) \\ & + \frac{H^{+^6}}{84}[2\theta_{11}(\omega_7 - 7) - 3(\theta_{12}\omega_5 - 2\theta_{13}\omega_6)] \\ & + \frac{H^{+^4}}{20}\{\theta_{12}(\omega_7 - 5) - 2[\theta_{13}\omega_5 + \omega_3(2\theta_7 - \Upsilon_4)]\} \\ & + \frac{H^{+^2}}{12}\{2\theta_{13}(\omega_7 - 3) + \theta_4\omega_2 \\ & +2[2\Upsilon_3\omega_2 - \Upsilon_4\omega_4 + \omega_3(\Upsilon_5 - 2\Upsilon_6)]\} \\ & - \frac{\Upsilon_1\omega_1 - \Upsilon_2\omega_2 + \Upsilon_5\omega_4}{2}.\end{aligned} \tag{40}$$

References

Afonso AM, Alves MA, Pinho FT (2009) Analytical solution of mixed electro-osmotic/pressure driven flows of viscoelastic fluids in microchannels. J Non-Newton Fluid Mech 159:50–63

Berli CLA, Olivares ML (2008) Electrokinetic flow of non-Newtonian fluids in microchannels. J Colloid Interf Sci 320:582–589

Berthier J, Silberzan P (2006) Microfluidics for biotechnology. Artech House, Norwood

Bird RB, Armstrong RC, Hassager O (1987) Dynamics of polymeric liquids. Vol 1: fluid mechanics. Wiley, New York

Bruus H (2008) Theoretical microfluids. Oxford University Press

Burmeister LC (1983) Convective heat transfer. Wiley, New York

Catenaccio A, Daruich Y, Magallanes C (2003) Temperature dependence of the permittivity of water. Chem Phys Lett 367: 669–671

Chakraborty S (2005) Dynamics of capillary flow of blood into a microfluidic channel. Lab-on-Chip 5:421–430

Chakraborty S (2007) Electrostatically driven capillary transport of typical non-Newtonian biofluids in rectangular microchannels. Anal Chim Acta 605:175–184

Coelho PM, Pinho FT (2009) A generalized definition of Brinkman number for duct flow. J Non-Newton Fluid Mech 156:202–206

Das S, Chakraborty S (2006) Analytical solutions for velocity, temperature and concentration distribution in electroosmotic microchannel flows of a non-Newtonian bio-fluid. Anal Chim Acta 559:15–24

Debye P, Hückel E (1923) Zur Theorie der Electrolyte I. Gefrierpunktserniedrigung und verwandte Erscheinungen. Physikalische Zeitschrift 24:185–206

Dutta A, Tarbell JM (1996) Influence of non-Newtonian behaviour of blood on flow in an elastic artery model. ASME J Biomech Eng 118:111–119

Easthope PL, Brooks DF (1980) A comparison of rheological constitutive functions for whole human blood. Biorheology 17:235–247

Elazhary A, Soliman HM (2009) Analytical solutions of fluid flow and heat transfer in parallel-plate micro-channels at high zeta-potential. Int J Heat Mass Transf 52:4449–4458

Horiuchi K, Dutta P (2004) Joule heating effects in electroosmotically driven microchannel flows. Int J Heat Mass Transf 47:3085–3095

Jendrejack RM, Dimalanta ET, Schwartz DC, Graham MD, de Pablo JJ (2003) DNA dynamics in a microchannel. Phys Rev Lett 91:038102

Koo J, Kleinstreuer C (2004) Viscous dissipation effects in microtubes and microchannels. Int J Heat Mass Transf 47:3159–3169

Larson RG (1999) The structure and rheology of complex fluids. Oxford University Press, Oxford

Mala GM, Li D, Dale JD (1997) Heat transfer and fluid flow in microchannels. Int J Heat Mass Transf 40:3079–3088

Maynes D, Webb BW (2004) The effect of viscous dissipation in thermally fully-developed electro-osmotic heat transfer in microchannels. Int J Heat Mass Transf 47:987–999

Moyers-Gonzalez MA, Owens RG, Fang J (2008) A non-homogeneous constitutive model for human blood Part III: oscillatory flow. J Non-Newton Fluid Mech 155:161–173

Nguyen NT, Wereley ST (2006) Fundamentals and Applications of microfluidics. Artech House, Norwood

Olivares ML, Vera-Candioti L, Berli CLA (2009) The EOF of polymer solutions. Electrophoresis 30:921–929

Ong CL, Owen JM (1991) Computation of the flow and heat transfer due to a rotating disc. Int J Heat Fluid Flow 12:106–115

Park HM, Choi YJ (2009) Electroosmotic flow driven by oscillating zeta potentials: comparison of the Poisson–Boltzmann model, the Debye–Hückel model and the Nernst–Planck model. Int J Heat Mass Transf 52:4279–4295

Park HM, Lee WM (2008) Helmholtz–Smoluchowski velocity for viscoelastic electroosmotic flows. J Colloid Interf Sci 317:631–636

Park HM, Lee JS, Kim TW (2007) Comparison of the Nernst–Planck model and the Poisson–Boltzmann model for electroosmotic flows in microchannels. J Colloid Interf Sci 315:731–739

Pinho FT, Coelho PM (2006) Fully-developed heat transfer in annuli for viscoelastic fluids with viscous dissipation. J Non-Newton Fluid Mech 138:7–21

Pinho FT, Oliveira PJ (2000) Analysis of forced convection in pipes and channels with the simplified Phan-Thien–Tanner model. Int J Heat Mass Transf 43:2273–2287

Russel WB, Saville DA, Schowalter WR (1991) Colloidal dispersions. Cambridge University Press, Cambridge

Soong CY, Wang SH (2003) Theoretical analysis of electrokinetic flow and heat transfer in a microchannel under asymmetric boundary conditions. J Colloid Interf Sci 265:202–213

Sousa JJ, Afonso AM, Pinho FT, Alves MA (2011) Effect of the skimming layer on electro-osmotic—Poiseuille flows of viscoelastic fluids. Microfluid Nanofluid 10:107–122

Stone HA, Stroock AD, Ajdari A (2004) Engineering flows in small devices: microfluidics toward a lab-on-a-Chip. Annu Rev Fluid Mech 36:381–411

Tang GY, Yang C, Chai CJ, Gong HQ (2003) Modeling of electroosmostic flow an capillary electrophoresis with the Joule heating effect: the Nernst–Planck equation versus the Boltzmann distribution. Langmuir 19:10975–10984

Tang GY, Yang C, Chai JC, Gong HQ (2004) Joule heating effect on electroosmotic flow and mass species transport in microcapillary. Int J Heat Mass Transf 47:215–227

Tang G, Yan D, Yang C, Gong H, Chai JC, Lam YC (2006) Assessment of Joule heating and its effects on electroosmotic flow and electrophoretic transport of solutes in microfluidic channels. Electrophoresis 27:628–639

Vick B, Özisik MN (1981) Effects of axial conduction and convective boundary conditions in slug flow inside a circular tube. ASME J Heat Transf 103:436–440

Wapperom P, Hulsen MA (1998) Thermodynamics of viscoelastic fluids: the temperature equation. J Rheol 42:999–1019

Yang C, Li D, Masliyah JH (1998) Modeling forced liquid convection in rectangular microchannels with electrokinetic effects. Int J Heat Mass Transf 41:4229–4249